UNCLASSIFIED

DEFENCE R&D DÉFENSE

Measurement of the Limit of Shock Precompression and Induction Delay Time of Liquid Explosives
(Final Report)

Dr. Andrew J. Higgins and Dr. John H.S. Lee
Swacer Inc.

Scientific Authority:
Dr. Fan Zhang
Defence Research Establishment Suffield

WARNING

"The use of this information is permitted subject to recognition of propretary and patent rights."

DEFENCE RESEARCH ESTABLISHMENT SUFFIELD

Contract Report
DRES CR 2001-045

February 2001

National Defence Défense nationale

Canada

UNCLASSIFIED

Measurement of the Limit of Shock Precompression and Induction Delay Time of Liquid Explosives

FINAL REPORT
for work carried out under Contract No. W7702-9-R747/001/EDM

Submitted to:

Dr. Fan Zhang
Defence Research Establishment Suffield
P.O. Box 4000, Medicine Hat
Alberta, Canada T1A 8K6

Submitted by:

Dr. Andrew J. Higgins
Dr. John H.S. Lee
SWACER Inc.
315 Querbes, Outremont
Québec, Canada H2V 3W1

December 27, 2000

Measurement of the Limit of Shock Precompression and Induction Delay Time of Liquid Explosives

FINAL REPORT
for work carried out under Contract No. W7702-9-R747/001/EDM

Submitted to:

Dr. Fan Zhang
Defence Research Establishment Suffield
P.O. Box 4000, Medicine Hat
Alberta, Canada T1A 8K6

Submitted by:

Dr. Andrew J. Higgins
Dr. John H.S. Lee
SWACER Inc.
315 Querbes, Outremont
Québec, Canada H2V 3W1

December 27, 2000

Executive Summary

This report presents the results of a one-year study into the shock initiation of detonation in liquid explosives. This study used nitromethane (both pure and chemically sensitized) as the test explosive. The initiating shock wave was generated by the detonation of sensitized nitromethane (the "donor"), which was attenuated by a gap of inert material before transmission into the test charge of nitromethane (the "receptor"). Considerable effort was directed at developing and assessing diagnostics that could be used to track the shock wave in the inert attenuator and measure or predict the shock pressures generated. The shock *x-t* trajectory in inert attenuator materials (PMMA and copper) were measured using shock pins and contact gauges with two different diameter charges (25 and 50 mm). Once the shock trajectory is measured, the shock velocity and known Hugoniot data were used to predict the shock pressure. These predictions were independently verified with direct measurement of pressure using manganin gauges, which also permitted the pressure profile behind the shock to be obtained.

Once the shock generator (donor charge and attenuator) were well quantified, the initiation of nitromethane (both pure and sensitized) was studied as a function of the strength of the transmitted shock and the diameter of the charge configuration. The critical thickness of PMMA attenuator was determined for charges of 25, 50, and 100 mm in diameters. These experiments were primarily "Go" or "No Go" tests, with the trajectory of the shock transmitted into the test explosive being monitored with shock pins along the wall of the charge. The results at different scale show that the diameter of the charge has a significant effect on the critical shock pressure required for initiation. This result is consistent with the fact that lateral rarefactions from the edges of the charge may retard or quench chemical reactions, thus preventing initiation. Preliminary comparisons of this charge diameter effect with fundamental shock initiation data (overtake time, etc.) are made, and the current results are consistent with previously published data.

Table of Contents

Executive Summary i
Introduction 1
Methodology 1

Part 1: Shock Wave Generator

1.1 Introduction 3
1.2 Diagnostics 3
1.2.1 Twisted Pair 3
1.2.2 Contact Gauges 4
1.2.3 Shock Pins 4
1.2.4 Manganin Gauges 4
1.2.5 Photodiodes 5
1.3 Assessment of Diagnostics 5
1.3.1 Charge Configurations 5
1.3.2 Results 5
1.4 Guidelines for Further Experiments 10
1.5 Planarity 12
1.6 Attenuation Measurements (PMMA) 14
1.6.1 Results with 25 mm Diameter Charges 14
1.6.2 Results with 50 mm Diameter Charges 16
1.7 Pressure in Attenuator (PMMA) 19
1.7.1 Pressure from Velocity Estimate 19
1.7.2 Direct Measurement of Pressure with Manganin Gauges 19
1.8 Results in Copper 21
1.8.1 Shock Trajectory 21
1.8.2 Manganin Gauge Measurements 24
1.9 Summary of Attenuation Data 24

Part 2: Shock Initiation of Liquid Explosives

2.1 Introduction 26
2.2 Procedure 26
2.3 Sample "Go" and "No Go" results 28
2.4 Results with Pure Nitromethane 29
2.5 Results with Sensitized Nitromethane 30
2.5.1 Results at 25 mm Scale 30
2.5.2 Results with Longer Donor (25 mm Diameter) 31
2.5.3 Results at Larger Scale 31
2.6 Analysis 34
2.6.1 Interpretation 35
2.6.2 Comparison to Published Data on Sensitized Nitromethane 36
2.7 Conclusions 39
Acknowledgements 40
References 40

Appendix A: Compatibility Tests with Nitromethane and DETA 41
Appendix B: Photodiode Circuit 50
Appendix C: Impedance Matching Calculations of Various Materials 51

Introduction

The shock sensitivity of an explosive is typically quantified by the strength and duration of the shock wave required to initiate it. Shock sensitivity is usually measured by the so-called "gap test" in which a slab of inert material is placed between a known explosive donor and the test explosive.[1] Varying the thickness of the inert layer or "gap" between the donor charge and the test explosive determines the strength of the shock wave transmitted into the test explosive. This gap thickness is varied until the critical thickness between detonation and no detonation occurs (typically, the tests are repeated until a statistically significant number of trials can be used to determine the gap thickness required for 50% Go" and 50% "No Go"). These tests have been standardized in terms of the donor explosive and diameters used (e.g., the U.S. NOL large-scale gap test uses 2 inch diameter charges).

These standardized explosive tests are in sharp contrast to experiments that focus on the phenomenon of shock initiation of explosives. Beginning with the early studies of Campbell, Davis, and Travis [2], shock initiation studies have involved using very large diameter plane wave generators (20 cm in Campbell's experiments) to generate a nearly ideal, one-dimensional shock in an inert attenuator that was then transmitted into the test medium. As research progressed, the diameter of the experiments increased to very large dimensions, e.g. Walker and Wasley used a 30 cm diameter plane wave generator to study the shock initiation of nitromethane by low-amplitude shock waves.[3] These pioneering studies did not report, however, the quantitative criterion used to determine the minimum charge size necessary to obtain effectively planar initiation. In short, how large does a "gap" test need to be in order to approximate an "ideal" planar shock initiation experiment?

This report details the results of an investigation into the shock initiation of a liquid explosive (nitromethane), with a particular emphasis placed on identifying the parameters that influence a finite-diameter "gap" test in comparison to an "ideal" experiment examining shock initiation of an explosive.

Methodology

In this study, experiments were developed using small-scale (25 mm diameter) charges and then scaled up to large diameter charges (50 mm and 100 mm diameter). Shock initiation experiments are typically performed with very large diameter donor charges (as large as 30 cm diameter) so as to eliminate the effect of lateral expansions and interactions with the test charge confinement.[2,3] This type of experiment can only be performed in large-scale blast chambers or in open field trials at considerable expense. Thus, all of the present experiments are developed at the 25 mm diameter scale in a small, laboratory-scale blast chamber, and only when confidence is obtained in the diagnostic technique is the experiment scaled up for large blast chamber or field trial experiments.

In addition to the expense of conducting field trials, experiments with shocks in condensed matter incur considerable expense due to the diagnostics used, which are destroyed with every test. Thus, these experiments were developed using the least expensive diagnostics

(e.g., contact gauges built in-house), then verified using commercially produced diagnostics (Dynasen shock pins). After the shock trajectory in the attenuator was measured, the shock pressure can be predicted from the known equation of state of the material, and then the prediction verified by select point measurements with manganin gauges (at $150 each).

A similar methodology was adopted for the shock initiation experiments: the experiments were performed extensively on the 25-mm-diameter scale before being scaled up to 50- and 100-mm-diameter charges.

Part 1: Shock Wave Generator

1.1 Introduction

A detonation front in a condensed explosive that impacts an inert layer (with the interface perpendicular to direction of detonation propagation) will transmit a shock into the inert material. The strength of this shock can be determined directly by impedance matching calculations, and in principle this shock propagates at constant speed. The effects of a finite sized charge, however, result in a decay in the shock velocity. For one, rarefactions propagating from the rear of the explosive charge (the so-called Taylor wave) overtake the transmitted shock and continuously lower the shock pressure and velocity. Also, if the charge is of a finite diameter, lateral rarefactions propagate into the shocked material, progressively lowering the shock pressure and velocity as they move inward, resulting in a curved shock front. If the explosive charge is point-initiated, then there is an additional mechanism of shock deceleration due to curvature of the front and unsteady expansion of the products behind the detonation. The attenuation of a shock in an inert material provides a means of varying the strength of shock that is transmitted into a test material. This is the basis of gap tests for explosive sensitivity.

This Section (Part 1) discusses the diagnostics available for tracking the shock wave in an inert material, assesses the proper use of these diagnostics, then proceeds to measure and quantify the shock wave transmitted through inert materials (PMMA and copper) at different scales.

1.2 Diagnostics

1.2.1 Twisted Pair

These probes consisted of two thin (0.24 mm) wires twisted about each other. The wires (transformer wire) are coated with a thin layer of insulating varnish. Upon shock compression, the insulation breaks down and the wires short, permitting passage of charge. The twisted pairs were used with a discriminator box that puts 15 Volts across the wires. This box uses an R.C. input circuit to generate a sharp but noisy signal. This signal is converted into a clean signal by a Schmitt trigger that is then locked by an analog memory block. Finally, the signal goes to a step generator that combines the output of several TP's as a series of steps with different amplitudes. This box is essential to eliminate the multiple signals generated by a single TP and the large amount of cross-talk between different TP's in the same experiment.

If the twisted pair is located on the interface between the NM and the PMMA attenuator, the probe is glued on the flat surface of the PMMA. For twisted pair probes located in the PMMA, probes are embedded in the surface of the PMMA disks by etching a small groove in the PMMA using a soldering iron. This ensures that the disks will properly stack with the TP wires between them.

Results obtained with a TP will be denoted with "X" in this report. Control experiments with "untwisted" twisted pairs (where the wires are not in physical contact) are denoted with "I."

1.2.2 Contact Gauges

These probes are similar to the TP's, but rather than insulated wires, they are comprised of brass foils (0.001", noninsulated, Small Parts Inc.) separated by a thin gap (0.003") of two-sided tape with a 0.25"-diameter hole in the center of the strip. Some experiments were performed with household aluminum foil, however this foil is easily creased and wrinkled and therefore is not as suitable for contact gauges as brass foil. The foils are connected to the same discriminator box as the TP's. Assuming a shock velocity of ≈3 km/s has a corresponding particle velocity of ≈1 km/s, then the time it takes the foils to close the 0.003" gap is on the order of 100 ns for these experiments.

These foils are made circular in shape with a diameter of about 1". They are sandwiched between the PMMA disks using a piece of two-sided tape on both sides. Thus, the total thickness of the CG is about 0.01".

Results obtained with a CG will be denoted with "○" in this report. Control experiments performed using CG's without the hole (thus preventing the foils from shorting) are denoted with "●".

1.2.3 Shock Pins

The shock pins used are commercially available piezoelectric pins supplied by Dynasen Inc. (Goleta, CA). The specific pin used is the CA-1135, in which the piezoelectric crystal is housed in a 0.064-inch brass tube in lengths between 1 to 3 inches. The pins are inserted into the PMMA attenuator disks vertically from the bottom though at 1/16" hole. The signal is monitored directly on a 300 MHz LeCroy digital oscilloscope. The shock pins are connected to the oscilloscope in high impedance input mode via BNC cables closed on their characteristic impedance (50 Ω) to avoid reflection losses.

Results obtained with a SP will, in general, be denoted with "■" in this report. Pins on the central axis of the attenuator will be denoted with "■", while off-axis probes will be denoted with "△". Shock pins that are staggered at different distances from the NM charge throughout the attenuator will be denoted with "◆".

1.2.4 Manganin Gauges

Manganin (copper/manganese/nickel/iron alloy) foil is a material that changes resistance nearly linearly with pressure, but has a very nearly constant resistance with changing temperature. If calibrated, these gauges provide a means of direct measurement of shock pressures. The gauges used here are commercially available from Dynasen Inc. (Goleta, CA). Two different types of gauges are used: 50 Ω (Dynasen Model MN4-50-EK) and 0.050 Ω (Dynasen Model MN10-.050-FEP/PTFE). The 50 Ω gauges are more sensitive

and have a calibrated response between 0.5 and 10 GPa. The low impedance 0.050 Ω gauges are less sensitive, but are calibrated up to 50 GPa.

1.2.5 Photodiodes

While not used with shock attenuation measurements in mind, experiments in which photodiodes observed (via 960 μm core simplex plastic fiber, Fiber Instrument Sales, Inc., Part F1-7527) the experiment from the bottom of the test charge looking "up" toward the donor/attenuator yielded a signal that can be correlated to shock passage through the attenuator (see discussion in Section 1.6.2 below). The photodiode circuit used here is described in Appendix B.

1.3 Assessment of Diagnostics

1.3.1 Charge Configurations

The different experimental configurations of explosive charge and attenuator are shown in Fig. 1. Configuration "A" was chosen to be an inexpensive simulation of a donor charge (e.g., planar wave generator) in which the diameter of the donor is greater than the diameter of the attenuator. The explosive charge is contained in a wax paper "Dixie®" cup 2.25 inches long. The blasting cap was centered in a cardboard cap on the cup and was lowered 1 cm into the charge for all tests. The cup and disks of attenuator material (PMMA) are held together with two-sided tape. The mass of explosive used in this configuration was 100 g of sensitized nitromethane (90 g NM + 10 g DETA).

The second configuration "B" was used due to concerns regarding the annular "lip" of explosive which sticks out over the edge of the attenuator disks in "A". In this configuration, the internal diameter of the charge matches the diameter of the attenuator (1 inch). The mass of explosive used was 27 g of NM + 10% DETA (i.e., 24.3 g NM + 2.7 g DETA). The charge was held in a 2-inch-long acrylic tube, which was sealed at the bottom with wax paper. Note that while nitromethane dissolves the acrylic tube, these experiments were performed quickly so that the donor explosive was not significantly affected.

The third type of charge used the same mass of explosive as "A" but was the same diameter as "B." This charge was used to determine which factor was responsible for the inconsistent results obtained between the "A" and "B" configurations. The explosive for "C" was contained in a 7.4-inch-long paper tube.

1.3.2 Results

The results of 12 repeated experiments (BNCH001 → 012) using the "A" configuration from Fig. 1 are shown in Fig. 2. A dashed line on the x-t diagram shows a trajectory with velocity 5.19 mm/ms, the shock velocity transmitted into PMMA by nitromethane detonation as predicted by impedance matching calculations.[4] The zero-time is defined by the signal of the first probe. Thus, all the points at the $x = 0$ location agree by definition. A few experiments were performed with both TP's and CG's at the $x = 0$

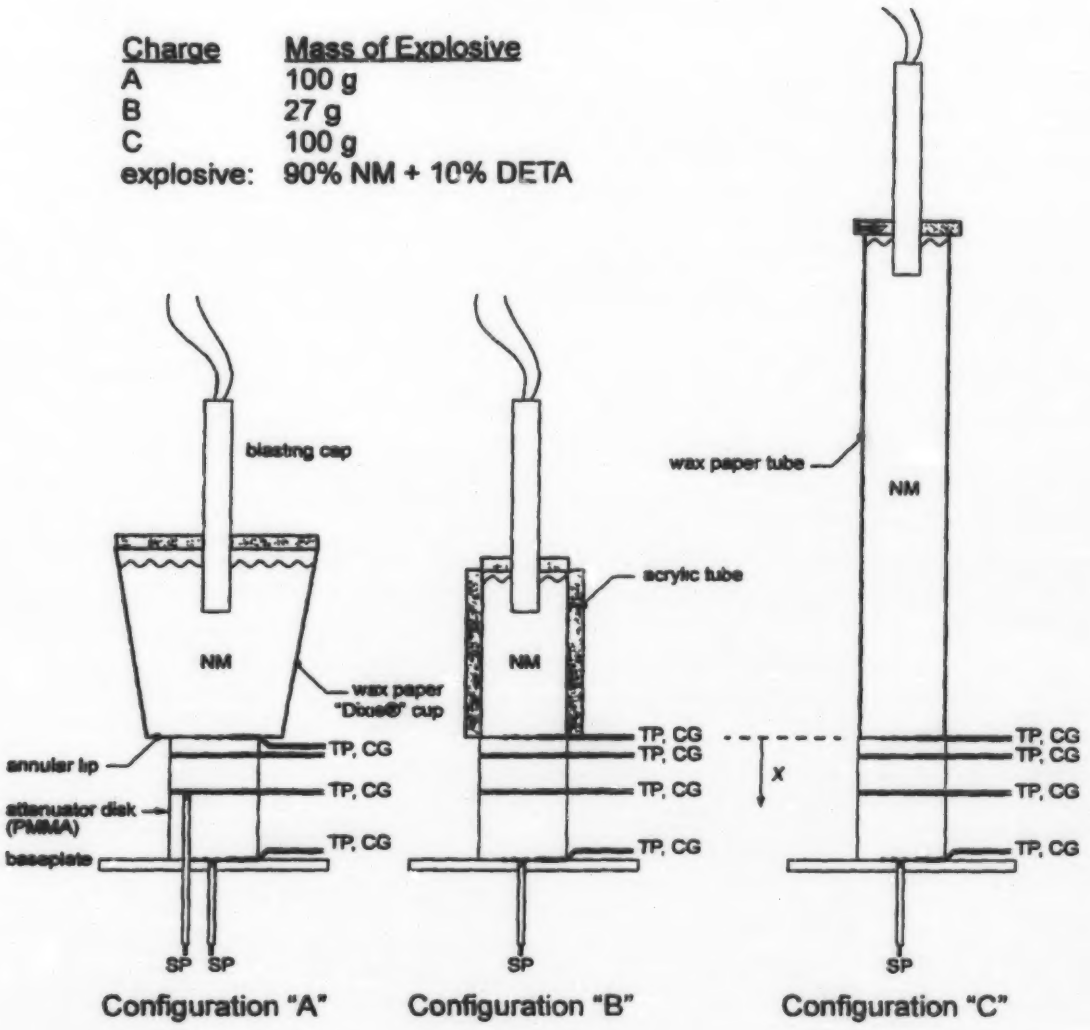

Fig. 1 Experiment configuration of charges used to validate diagnostics for shock waves in PMMA.

location. The signals from both probes at that location were in good agreement, although a difference of 200 ns was obtained for one experiment. The signals at the $x = 5$ mm location also agreed very well. As the shock propagated farther into the PMMA, however, the scatter in time of arrival increased significantly.

Note that at the $x = 35$ mm location, there is a very wide range of shock wave time of arrival (TOA), between 4 and 12 μs. This represents a very large scatter in shock wave velocity and decay rate. Further note that, in at least one experiment, a TP showed the shock wave actually *accelerating* in PMMA to velocities greater than the detonation velocity of NM, and several additional experiments with CG's and TP's showed the shock

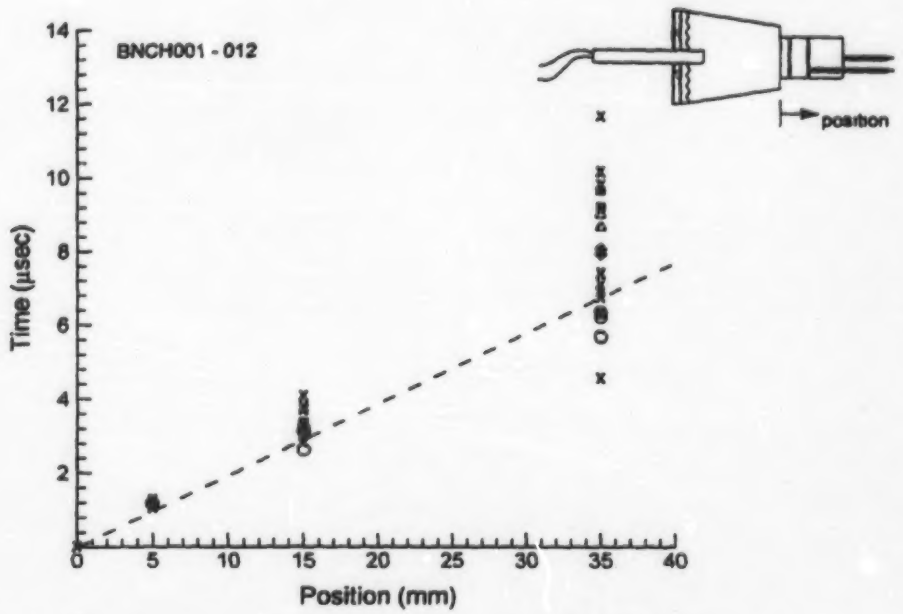

Fig. 2 Experiments with charge configuration "A" (cf. Fig. 1). Dashed line is shock trajectory from impedance matching calculation.

X Twisted pair

○ Contact gauge

■△◆ Shock pin

wave propagating at constant velocity (no decay). These are obviously nonphysical results.

It was speculated that the annular "lip" of explosive that extended beyond the attenuator disks in configuration "A" of Fig. 1 resulted in a jet of explosive products that propagated down the outside of the attenuator. The interaction of this jet with the wire leads extending from the TP's and CG's could have resulted in signals from these probes before the arrival of the shock wave. The particle velocity behind a detonation front in a condensed explosive is about half the detonation velocity, but the velocity of particles in a free expansion from a surface is about twice their initial velocity. Thus, the detonation products should expand from the free surface of the lip in Configuration "A" at about 6 km/s, which is consistent with the velocities obtained with the side-mounted probes.

Support of this theory comes from the SP's; since the lead wires from the SP's emerge from the bottom of the attenuator disks, rather than the side, they should be immune from this jetting effect. Indeed, in Fig. 2, the shock pins are not observed to give acceleration or constant velocity shock waves. The TOA of the shock pins at the $x = 35$ mm location, however, still exhibited a large amount of scatter (7.9 µs to 9.7 µs).

It was speculated that the scatter in TOA as measured by the SP's was due to a precursor shock transmitted through the shock pin material (brass) of an earlier probe. Strong

evidence of this effect is seen in Fig. 3, where experiments using a single pin (■) at $x = 35$ mm are differentiated from experiments which had two shock pins (one at $x = 15$ mm and the other at $x = 35$ mm), denoted by ◆. Note that at $x = 35$ mm, experiments with multiple shock pins consistently registered an earlier shock. This is likely due to the fact that the longitudinal speed of sound for brass is 4.7 km/s, much greater than that for PMMA (2.7 km/s). While the shock transmitted through the pin was very likely weak, the typical "binary" response of the SP's prevents them from being able to differentiate the precursor shock from the main shock in the PMMA. In light of this result, further experiments (BNCH013 and onward) used only *single* shock pins or multiple shock pins *at the same location* to prevent any influence on later pins.

Since the annular lip of explosive in configuration "A" was suspected of contaminating results with CG's and TP's, configuration "B" from Fig. 1 was used, in which the explosive was contained in an acrylic (PMMA) tube whose internal diameter very closely matched the outside diameter of the PMMA attenuator disks. The smaller diameter charge results in using about a fourth of the explosive (27 g for "B" as opposed to 100 g for "A"). The results of experiments using this configuration are shown in Fig. 4. Note that, as compared to Figs. 2 and 3, a much "tighter," more reproducible, shock decay curve is obtained, providing further evidence that the "lip" of explosive in configuration "A" was responsible for the wide range of results in Figs. 2-3. Note also that although TP's were located at $x = 35$ mm in several of the experiments, no signals were obtained there at times less than 10 μs. This suggests that, by that distance into the attenuator, the shock wave has decayed to a strength where it is no longer capable of shorting the TP's. At earlier locations ($x < 20$ mm), the TP's agree well with the CG's. The CG's are apparently reliable, as they agree very well with the SP's, even at the $x = 35$ mm location.

To further confirm the role of the annular lip in configuration "A," a series of control experiments were performed with "untwisted" TP's and "no-hole" CG's. These probes should not give a signal if they are operating in the way intended, since the wires and foils cannot short. The results of these experiments using the "A" configuration are shown in Fig. 5. Note that the untwisted TP's (|) and the no-hole CG's (●) *did* give signals and that these signals suggest a shock wave that is, in some cases, propagating at constant velocity. This result provides further evidence that configuration "A" gives nonphysical results, since the probes in these experiments should have returned no signal at all or at least delayed signals.

If "no-hole" CG's are used in configuration "B", they also give a signal (see Fig. 6), but the signal occurs much later than the actual shock wave arrival time as measured by CG's and SP's. Thus, while CG's in configuration "B" are also apparently susceptible to spurious signals, these signals occur late and thus will not confuse the results returned from regular CG's.

An alternative explanation for the above results is that the nonphysical signals obtained with configuration "A" is a result of the larger amount of explosive used, not the annular lip. For example, the greater amount of EM noise could result in the anomalous early signals from the TP's and CG's. To rule out this possibility, a third configuration ("C" in Fig. 1) was used, which had the same mass of explosive as "A" (100 g) but had the same diameter (25 mm) as "B". This resulted in a charge of NM approximately 7.4" long. The

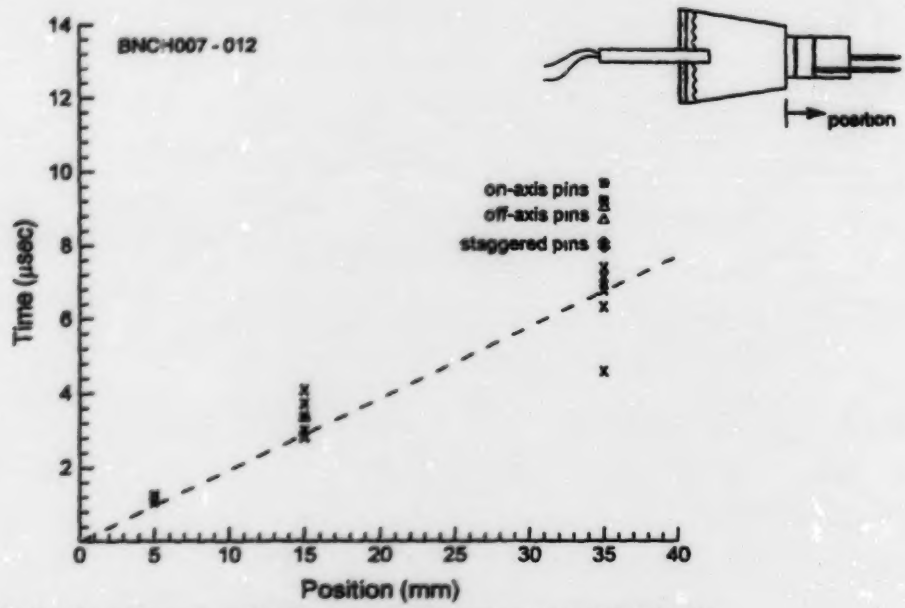

Fig. 3 Experiments with charge configuration "A" (cf. Fig. 1).
X Twisted pair
■△ Shock pin (on/off axis)
◆ Staggered shock pin

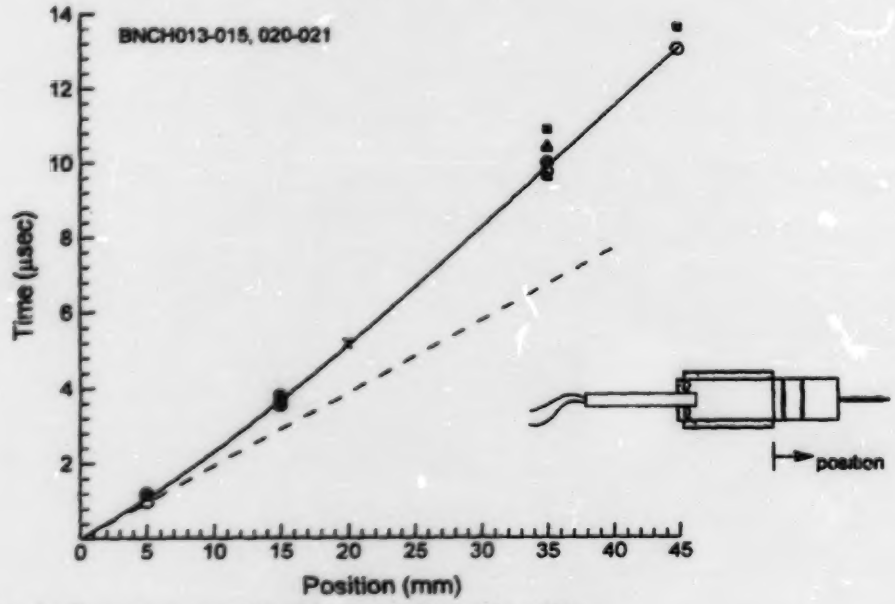

Fig. 4 Experiments with charge configuration "B".
X Twisted pair
○ Contact gauge
■△ Shock pin (on/off axis)

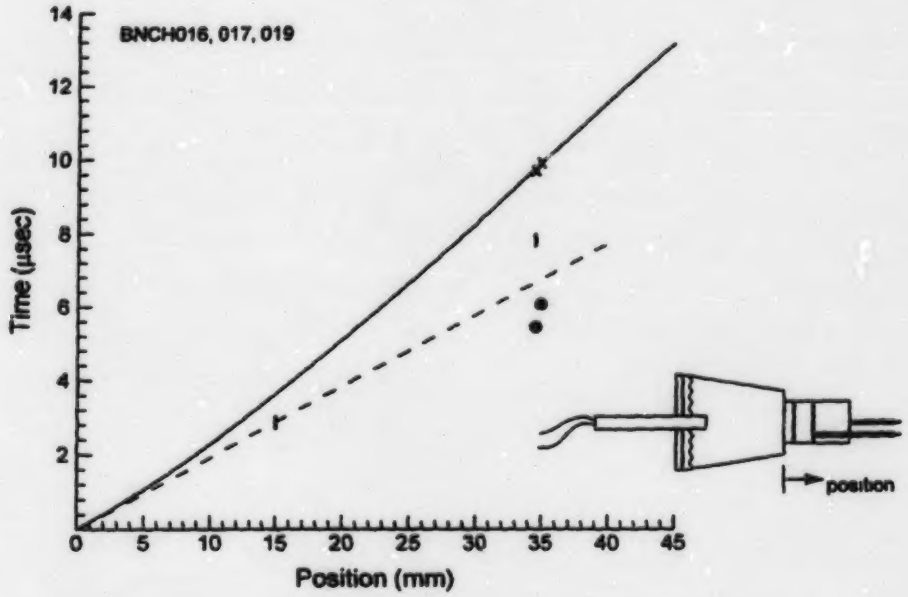

Fig. 5 Experiments with charge configuration "A" and gauges that should not give a response.
X Twisted pair
I Un-twisted pair
● Contact gauge with no hole

results with this longer charge are compared with the standard "B" configuration in Fig. 7. A curve fit of the data from configuration "B" is also shown (see Fig. 4 for source of this curve fit). Note the there is no discernible difference in the results between "B" and "C." This strongly suggests that the nonphysical results obtained with the "A" configuration were due to the wider diameter of the charge, not the larger amount of explosive used.

The results in Fig. 7 also have another interesting implication: the fact that the data with the "C" configuration agrees so well with the curve fit of the "B" configuration results shows that the attenuation of the shock is not influenced as the length of the explosive charge is increased by a factor of almost 4 (from 2" to 7.4"). This implies that the shock attenuation is not due to rarefactions resulting from the finite length of the charge, but rather from lateral rarefactions due the finite diameter of the charge and attenuator. The ability of the transmitted shock to initiate a test explosive from these two different lengths of donor will be compared in Section 2.3.2.

1.4 Guidelines for Further Experiments

The explosive used to drive a shock wave into the attenuator or test material should not be larger in diameter than the attenuator or test material. The exposed "lip" of explosive gives rise to a free jet of explosive products that expands down the side of the material faster than the shock wave inside the material. If probe leads are located on the outside of

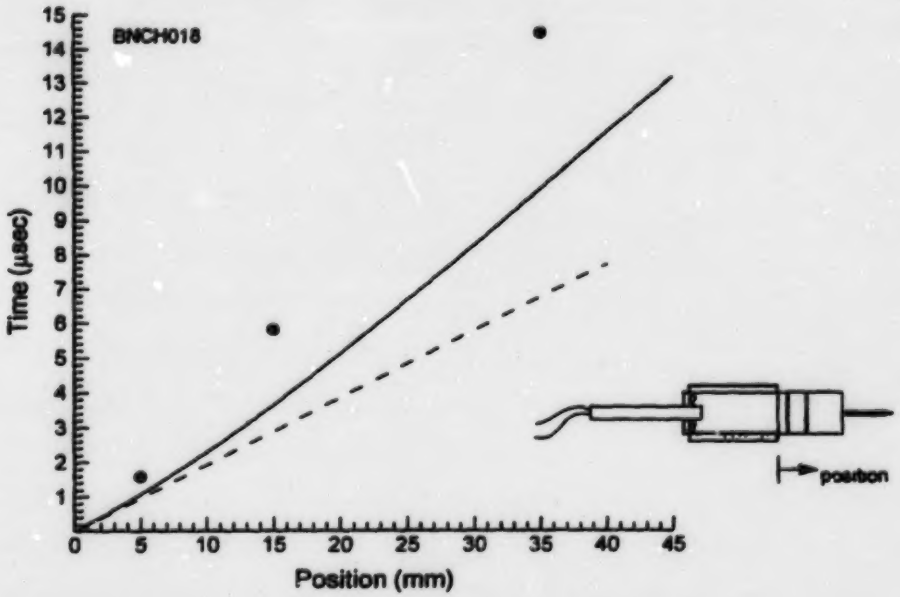

Fig. 6 Experiments with charge configuration "B" and gauges that should not give a response.
● Contact gauge with no hole

the charge, this jet can result in false readings that show a shock wave propagating faster than it actually does. This phenomenon is remarkably regular and could easily be confused with an accelerating or other anomalous shock. This problem was eliminated when the charge diameter was made equal to the attenuator diameter. Another solution would be to use a "shield" of material around the lip to prevent the detonation products from jetting down the sides of the attenuator. The standard practice, however, is to simply make the attenuator and shock compression experiment larger to match the larger PWG, but to only use the central section of the experiment to maintain maximum planarity.

Shock waves can be transmitted through shock pins faster than the shock wave propagates through the material of interest. Thus, if shock pins are inserted axially into the attenuator, the later pins will register a shock that was transmitted by the earlier pins, again giving the appearance of an accelerating or anomalously fast shock wave. While the hole for the shock pins could be made larger in an attempt to prevent the shock in the pin material from being transmitted back into the surrounding attenuator material, it will be difficult to ensure that the pin is centered in the hole without touching the walls. The simplest solution is to simply limit one pin per experiment, or if several pins are used, to locate them at the same distance from the charge.

It appears that CG's are a reliable instrument that can be used to complement SP's for time-of-arrival measurements. TP's are reliable for high shock pressures near the explosive charge, but do not respond at lower pressures. They are ideal to provide a trigger or reference time when in direct contact with the explosive, but should not be used to track shocks in inert solids.

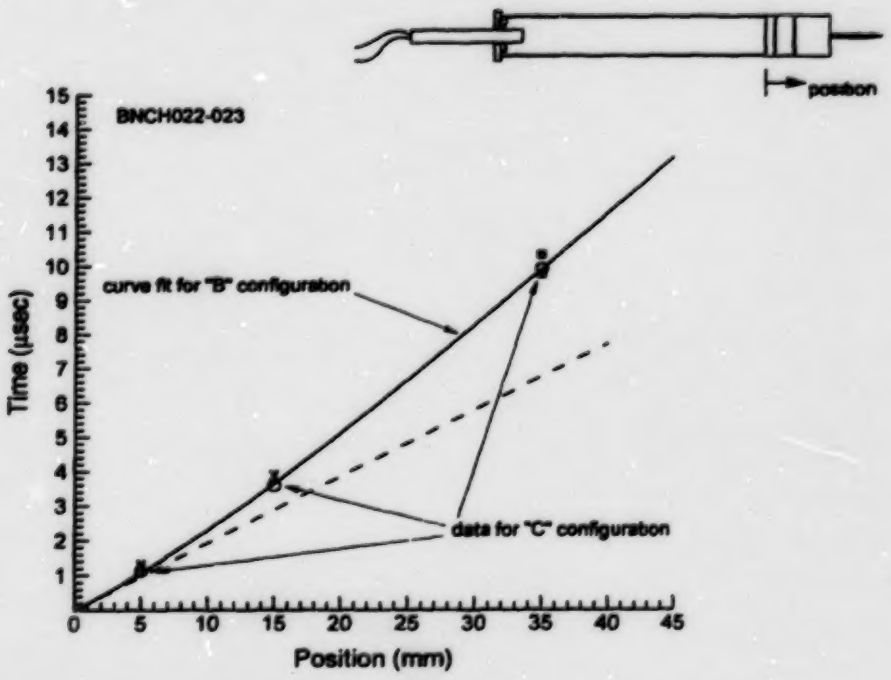

Fig. 7 Results with configuration "C", compared to curve fit for "B" configuration (cf. Fig. 4).
X Twisted pair
O Contact gauge
■ Shock pin

To summarize, the results here provide the following guidelines in how to conduct shock attenuation experiments:

- Avoid charge configurations where jetting of explosive products onto diagnostics is possible.
- Use only one shock pin per shot.
- Twisted pairs are not good for shocks in inert materials, TP's are only good when in direct contact with the detonation.
- Shock pins are the best instrument for shock arrival, but contact gauges provide an inexpensive independent check.

These guidelines are strictly adhered to for the rest of the results in this report.

1.5 Planarity

It is anticipated that large-scale shock compression experiments will use plane wave generators (PWG), obtained commercially or built in-house. For the small-scale

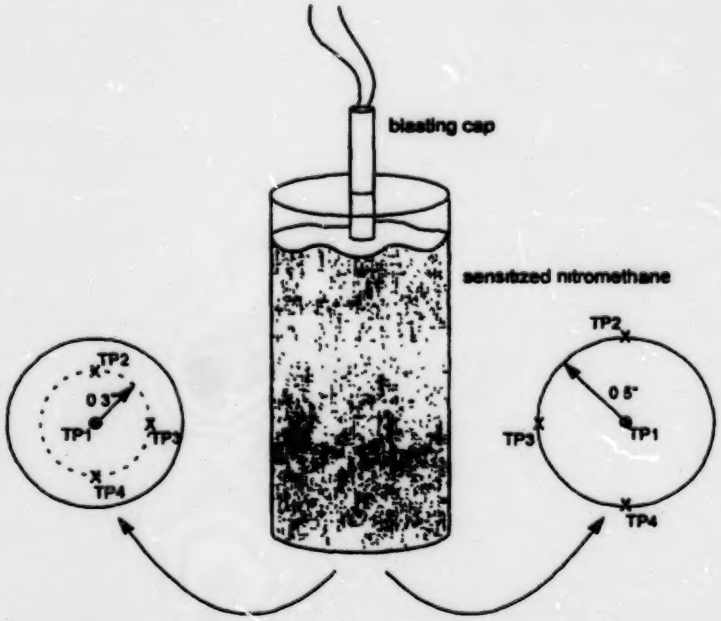

Fig. 8 Experiments to determine the planarity of detonation in a cylindrical charge of nitromethane.

benchmark experiment, it was uncertain whether a PWG was necessary or not. The use of a PWG adds considerable complexity and cost to the preparation of each charge. To determine the optimal design of the PWG (cone angle, point of initiation, etc.) would require considerable effort that would not necessarily carry over to the development of a larger scale PWG. Thus, a few experiments were conducted to see if a cylindrical charge of NM initiated at one end with a blasting cap would yield a detonation wave sufficiently planar for these preliminary experiments.

Two experiments using configuration "B" were conducted (PT001–002). The base of the nitromethane charge was instrumented with an array of twisted pairs (TP's), as shown in Fig. 8. The first experiment used TP's located 0.3" from the main axis of the charge; in the second experiment, they were located 0.5" from the axis, placing the TP's on the perimeter.

The results of these two experiments showed that from the center to 0.3" from the center, the difference in arrival time of the detonation was less then 120 ns, corresponding to a physical nonplanarity of 0.7 mm. At the perimeter of the charge, the arrival time from center to edge varied by 340 ns, corresponding to 2 mm in nonplanarity over the 25 mm diameter of the charge. These values agree well with simple kinematic estimates of the nonplanarity expected for a spherically expanding detonation after propagating 2" (the length of the charge).

It is worth pointing out that the response time of the step-generator box used to power the TP's is on the order of 50 ns. Thus, the difference in arrival time is approaching the

diagnostic resolution capability. This fact makes developing a PWG with better planarity difficult. Simply put, the nonplanarity of the simple, cylindrical charge is already at the threshold of detection, so there is little point in trying to develop a technique to deliver a more planar wave at this time.

1.6 Attenuation Measurements (PMMA)

Based on the findings in Section 1.2 and an extensive study of material compatibility (see Appendix A), the charge configuration used for the rest of the attenuation experiments and the shock initiation experiment in Section 2 was finalized. The design of this charge is shown in Fig. 9. Unless otherwise noted, the donor charge was a PVC capsule with a length twice the diameter. The detonator was centered in the top of the charge by a PMMA lid with a hole precision machined for the detonator (note that this PMMA lid does not come in contact with the NM donor). The donor explosive was nitromethane sensitized with 10% DETA. The PMMA attenuator was "snap-fit" into a lip machined into the PVC capsule. The PMMA attenuator was painted with manifold paint and, after being snapped into place, was covered with a thin layer of Pébéo drawing gum (see Appendix A). A twisted pair (TP) was centered on the attenuator, with the ends of the wires passing though small holes drilled in the PVC and then sealed with silicone. It was found that NM could short the TP's, so it was necessary to keep the ends of the TP's outside the liquid and protect the TP's by coating them with Pébéo drawing gum. The shock pin for determining shock arrival time was centered on the bottom of the attenuator, usually by a hole in the plate below the attenuator. Contact gauges were also used, and in some cases, multiple contact gauges were used in each experiment, sandwiched between PMMA disks.

1.6.1 Results with 25 mm Diameter Charges

The result of approximately 30 experiments examining shock attenuation in PMMA using 25 mm diameter charges is shown in Fig. 10. No data from Section 1.2 is used, as those results were not precision-machined charges with accurate placement of the gauges; only data obtained with the finalized configuration (Fig. 9) are used here.

Note that the results with shock pins are consistently earlier than the contact gauges by a time of a few hundred ns. This verifies the assumption that shock pins have a faster response. The time of shock arrival as measured by the "start of rise" of manganin gauge signals is also plotted as ♦.

While the data in Fig. 10 appears very consistent (the three shock pins at the 10 mm location agree to within less than 100 ns), the difficulty in using this data to determine the shock pressure in the attenuator comes when we attempt to determine the shock velocity by curve fitting and differentiating the x-t data. Three different curve fits of the shock pin and manganin data (contact gauges data excluded) in Fig. 10 were performed: (i) a 3rd order polynomial (shown in Fig. 10) (ii) 4th order polynomial and (iii) a 3rd order polynomial of the data in the $x = 0 - 15$ mm range (in Section 2, only attenuator thicknesses less than 15 mm are used, so this last curve fit is in the region of interest for interpreting the shock initiation experiments). A subtle but important point in curve fitting

Characteristic Charge Dimension	PVC Capsule Inside Diameter D_{inner}	PVC Capsule Wall Thickness (Schedule 80 Gray PVC)	Attenuator Diameter
25 mm	24. mm / 0.95"	4.6 mm / 0.18"	25 1 mm / 0 99"
50 mm	49. mm / 1.91"	5.6 mm / 0.22"	51.1 mm / 1.99"
100 mm	96 mm / 3.78"	9.0 mm / 0 35"	100.8 mm / 3.96"

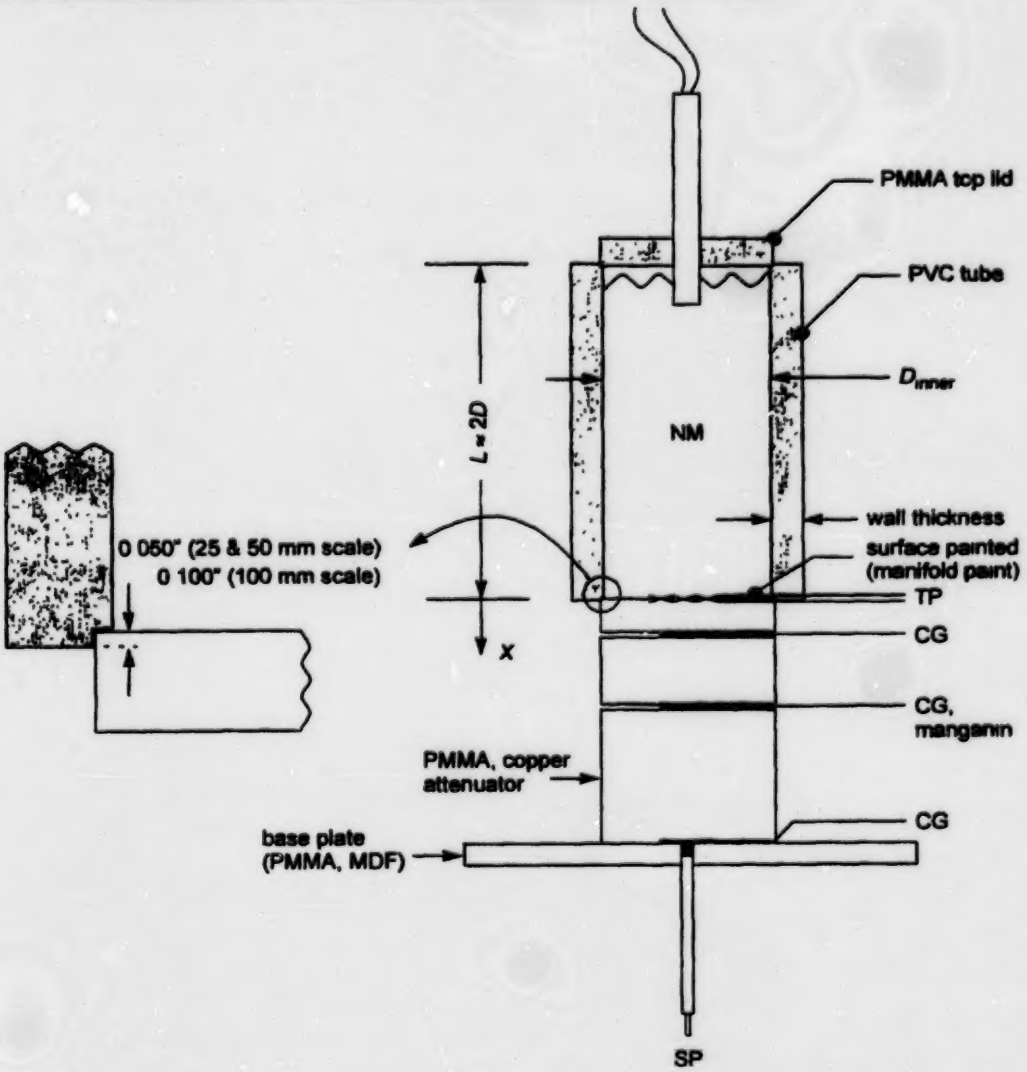

Fig. 9 Finalized configuration of donor for attenuation and initiation experiments (25, 50, and 100 mm scale).

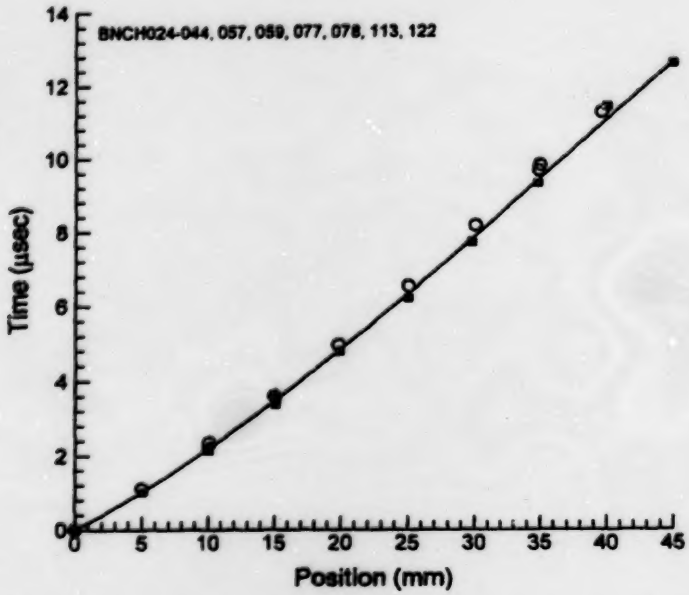

Fig. 10 Shock wave trajectory in 25 mm diameter PMMA attenuator, with 3rd order polynomial curve fit of shock pin and manganin data.
- ○ Contact gauge
- ■ Shock pin
- ◆ Manganin time of arrival

is that *each* experiment produces a data point at $x = 0$, with the time of arrival (by definition) $t = 0$. This point is recorded for each shot, and has the effect of "weighting" the $x = 0$, $t = 0$ point when least squares fitting the data in the x-t diagram. When these curve fits are differentiated to obtain velocity, the resulting velocity profiles are shown in Fig. 11. Note that while the x-t data appears very consistent in Fig. 10, there is considerable variation in the velocity obtained from curve fitting and differentiating that data. Since the 4th order curve fit produces a nonphysical oscillation in velocity near the ends of the attenuator, we will exclude this higher order curve fit here and will only use third order curve fits of the remaining experiments. Both of the 3rd order curve fits agree well, and match the ideal shock velocity at the NM/PMMA interface (5.2 km/s) as predicted by impedance matching calculations.[4] Thus, 3rd order fits will be used throughout the rest of this report. This means that, by definition, all of the V-x and P-x profiles will be quadratic.

1.6.2 Results with 50 mm Diameter Charges

The x-t data obtained with 50 mm and 100 mm charges is shown in Fig. 12. The 3rd order curve fit of the x-t data for the 25 mm charges (as determined in Section 1.4.1) is also shown for comparison. Note that due to the limited number of experiments that were

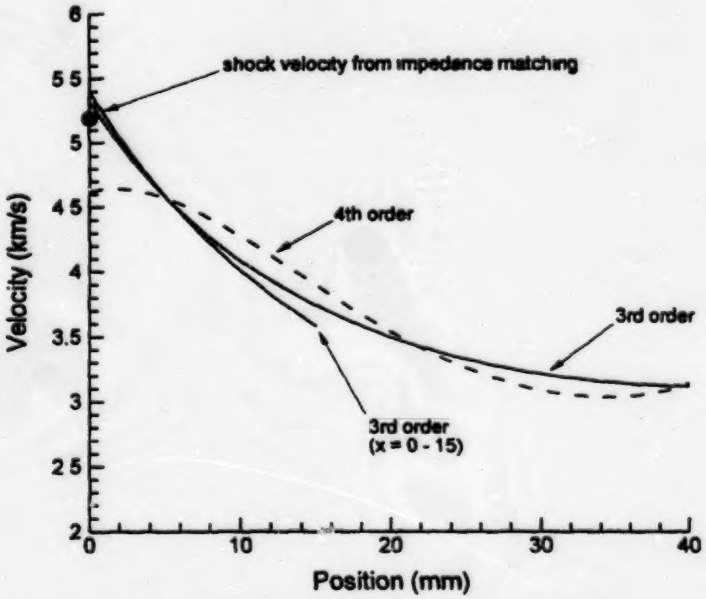

Fig. 11 Shock velocity in 25 mm diameter PMMA, obtained from differentiating various curve fits of *x-t* data (cf. Fig. 10).

performed at the 50 mm scale, contact gauges were predominately used, since multiple data points could be collected in a single experiment. Also shown are optical measurements of the shock arrival. These measurements were an interesting and unexpected result of having sheets of 2-sided tape sandwiched between disks of PMMA comprising the attenuator. A photodiode looking "upward" though a test charge of nitromethane (see charge configuration in Fig. 20) showed a series of sharp "spikes" in the intensity of luminosity, as shown in Fig. 13. A photomultiplier with the same view showed a series of "kinks" at approximately the same time, although the photodiode consistently lagged the photomultiplier by ~100 ns. Note that the photodiode is monitored with a differentiating circuit (see Appendix B) that results in an output that is more sensitive to changes in light intensity. If we interpret these spikes and kinks as the passage of the shock wave through the interface between PMMA disks (perhaps tearing the tape to permit more light through), then this result provides another independent means of measuring shock time of arrival. The photomultiplier measurements (denoted with an "L" in Fig. 12) agree very well with the conventional means of measuring shock wave time of arrival, so they are included in the data that is curve fit to obtain velocity and pressure.

The *x-t* trajectories for the 25 mm and 50 mm charges agree very well until about 15 mm into the attenuator, when the shock in the 25 mm attenuator begins to lag behind the shock in the 50 mm attenuator. This distance into the attenuator corresponds to approximately one charge radius at the 25 mm scale, at which point rarefactions from the edge of the charge reach the center, increasing the rate of shock deceleration.

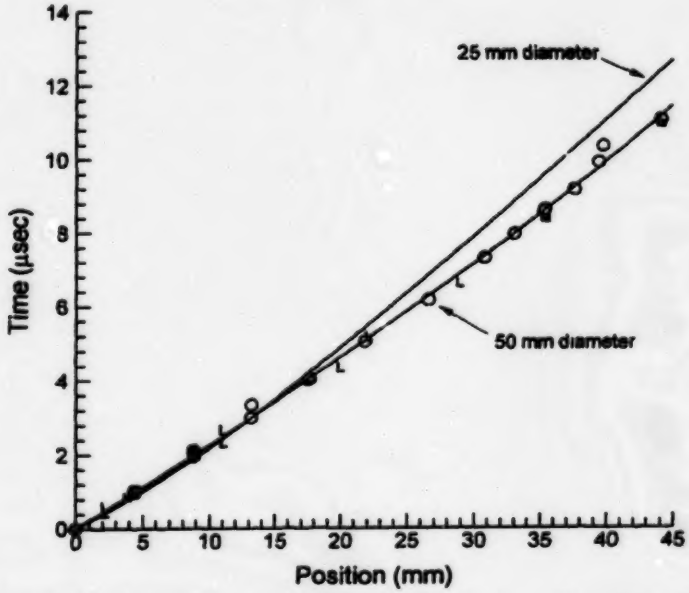

Fig. 12 Shock wave trajectory in 50 mm diameter PMMA attenuator, with 3rd order polynomial curve fit of the data.

O Contact gauge

■ Shock pin

L Luminosity signal (cf. Fig. 13)

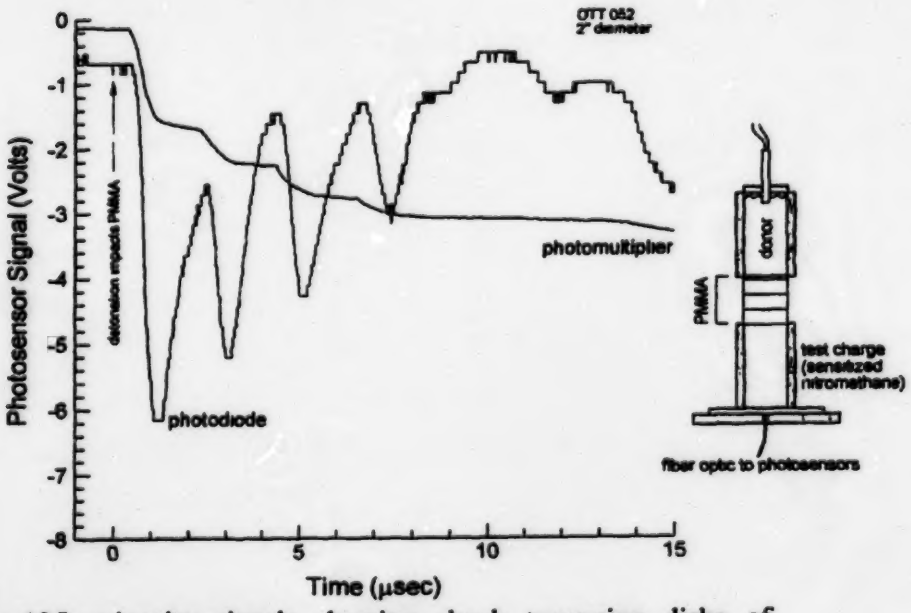

Fig. 13 Luminosity signals showing shock traversing disks of PMMA. Time of kinks plotted as "L" in Fig. 12.

Note that at present there is no data for shock attenuation with 100 mm diameter charges. However, the results at 25 and 50 mm suggest that the diameter of the charge does not affect the strength of the shock transmitted into the attenuator until it has propagated at least one charge radius into the attenuator. In Part 2 of this report, the attenuators used in shock initiation experiments at the 100 mm scale are approximately 30 mm thick, so that the shock attenuation and pressure at this thickness should be nearly the same as in the 50 mm charges. Thus, the attenuation data for the 50 mm charge will be used for the 100 mm diameter experiments.

1.7 Pressure in Attenuator (PMMA)

1.7.1 Pressure from Velocity Estimate

Using 3rd order curve fits of the *x-t* data for shock arrival in the 25 mm (using shock pins only) and 50 mm scale (using shock pins, contact gauges, and optical measurements), the velocity of the shock in the attenuator can be estimated. Using the known equation of state of PMMA, this velocity can be converted into a measurement of the peak shock pressure, as shown in Fig. 14. Using two different equations of state for PMMA:

$U_{shock} = c_0 + s\, u_{particle}$

Cooper [5]: $c_0 = 2.598$ km/s $\quad s = 1.516$

Batsanov [6]: $c_0 = 2.510$ km/s $\quad s = 1.545$ (valid P = 5-19 GPa)

yields nearly identical results; the curve fitting and differentiating of the *x-t* data result in much greater uncertainty in shock pressure than does the choice of Hugoniot: Note that while the "local" and "global" 3rd order curve fits of *x-t* data at the 25 mm scale produce consistent pressure profiles through the attenuator, curve fits of the 50 mm data over the entire domain and just over the region of interest to shock initiation experiment (x = 10 to 40 mm) yields pressure curves with significantly different slope. This discrepancy is likely due to the fact the contact gauges were the predominant diagnostic used in the 50 mm scale experiments, and these gauges do not produce as consistent shock time of arrival data as shock pins. Fortunately, the critical thicknesses of PMMA for both the 50 and 100 mm shock initiation trials (discussed in Part 2) are near 30 mm, where the two different curve fits are in good agreement. The shock pressure at this location is also directly measured using manganin gauges, as discussed below, providing further confidence in the value used. Thus, while the shock attenuation measurements at the 50 mm scale cannot be considered complete, the present results are sufficient to estimate the critical shock pressure for initiation experiments at 50 and 100 mm in Part 2 of this report.

1.7.2 Direct Measurement of Pressure with Manganin Gauges

The use of manganin gauges permits direct measurement of the shock pressure as well as the post-shock pressure profile. Manganin gauge measurements with 25 mm scale experiment are shown in Fig. 15, with gauges located at x = 10 mm and x = 15 mm. The

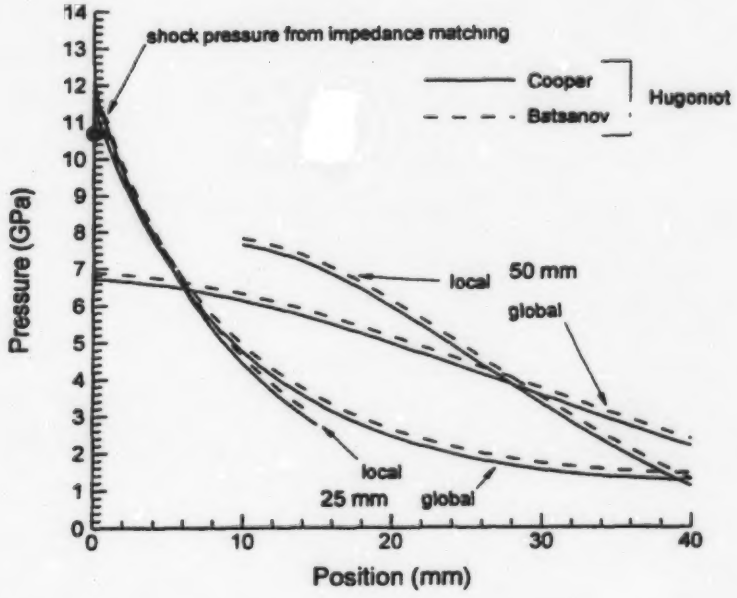

Fig. 14 Shock pressure in 25 mm and 50 mm diameter PMMA, obtained from differentiating various 3rd order curve fits of *x-t* data (cf. Fig. 12) and using the Hugoniot data of Cooper[5] and Batsanov[6]. Both global (incorporating all data) and local (just in region of interest for initiation) curve fits are used.

gauges at 10 mm are 0.050 Ω gauges, and being less sensitive they give a more noisy signal. The gauges at 15 mm are 50 Ω gauges and have a much better signal to noise ratio. Note that *two* experiments are shown for each location, with good reproducibility. The signals are truncated at less than 1 μsec after shock passage, due to the signal giving either a nonphysical gradual rise in pressure or a sudden jump in voltage due to the gauge breaking and the circuit going "open." The gradual rise in pressure after the shock is suspected to be an artifact of a nonplanar shock, and the transverse stretching of the gauge in the divergent flow behind the shock giving a false increase in pressure. Note that one of the gauges at the $x = 15$ mm location survived significantly longer than 1 μsec; the entire gauge in this experiment was protected by sheets of PMMA on both sides of the gauge, not just over the 25 mm diameter attenuator. It appears that protection of the manganin gauge is essential to having it survive for long period of time.

Also shown in Fig. 15 is one manganin measurement made with a 50 mm diameter charge, with the gauge placed at 28 mm into the attenuator (note that this experiment was performed with a primitive planar wave generator and booster charge configuration). Note that the effect of scale on shock attenuation may be seen: the peak shock pressure in the large diameter charge is greater, even though the gauge is located almost twice as far from the explosive/attenuator interface.

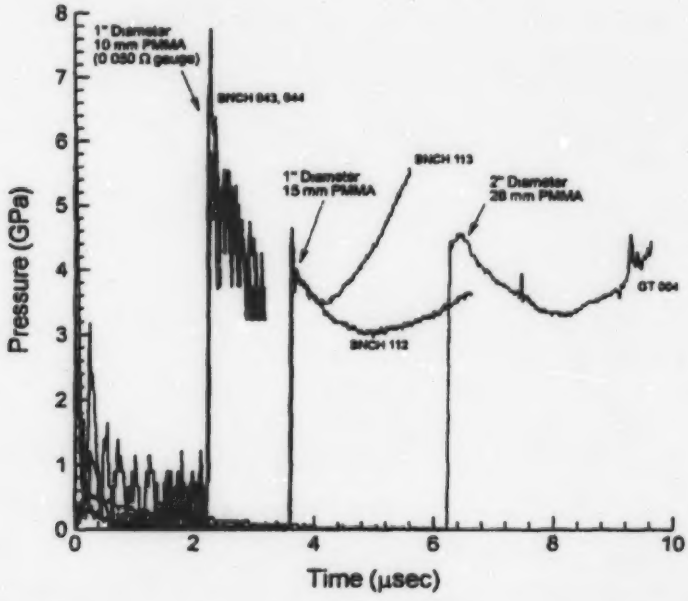

Fig. 15 Pressure profile in 25 mm and 50 mm diameter PMMA attenuators as measured by manganin gauges. Note that the 0.050 Ω gauge has lower sensitivity, resulting in a poor signal-to-noise ratio.

The shock pressures as measured by manganin gauges are compared to the estimated shock pressure using the *x-t* data in Fig. 16. Note that the manganin signals in Fig. 15 do not always have well defined peaks, so there is some interpretation involved in selecting the peak shock pressure. Nonetheless, the measured and estimated shock pressure are in reasonable agreement, with the values usually within 10% of each other. While the measurements here can be further refined with more shock pin measurements of shock trajectory, especially at the 50 mm scale, the overall approach of estimating shock pressure from the measured wave velocity appears valid.

1.8 Results in Copper

1.8.1 Shock Trajectory

All of the results discussed so far involve the use of PMMA as the inert attenuator. Since shock initiation experiments may involve the use of inert materials of higher impedance (e.g., in order to "split" the shock by density gradient, or as a "stiff" anvil for reflecting a shock), it is important that the diagnostics developed here can also be applied to these materials as well. For this reason, the attenuation measurement techniques described above were repeated with copper at the same scale (25 mm).

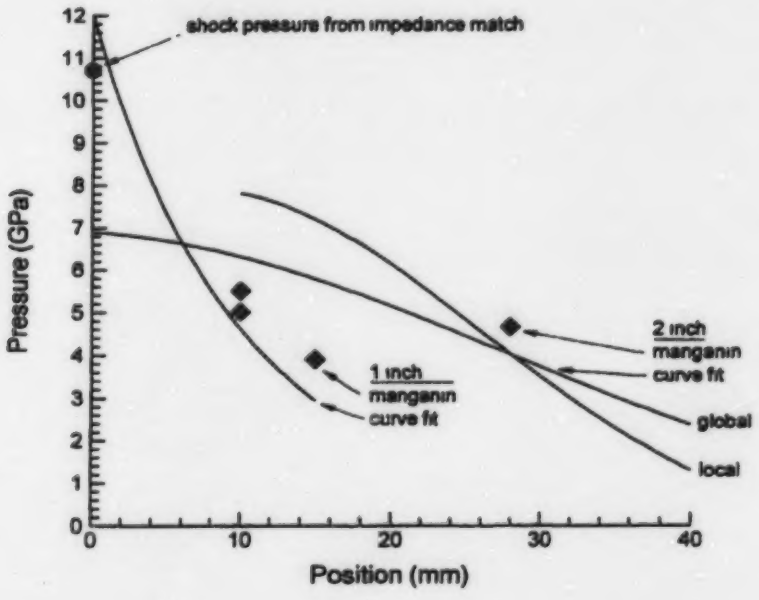

Fig. 16 Shock pressure in 25 mm and 50 mm diameter PMMA, obtained from differentiating curve fits of *x-t* data (cf. Fig. 12) and direct measurement via manganin gauges (cf. Fig. 15).

An interesting result of these experiments was the presence of an elastic precursor ahead of the shock, as detected by the shock pins. The "raw" shock pin signals from these experiments are plotted in Fig. 17. The amplitude of the signal in volts is shown, and each trace is offset from the prior one by the thickness of copper between measurements (usually 5 mm between successive pins). Again, only one shock pin is used per experiment to prevent one shock pin from interfering with the others. The signals clearly show the main shock splitting into a faster, weaker elastic precursor wave and a slower plastic shock. This phenomenon is to be expected whenever the shock pressure is on the order of the Hugoniot Elastic Limit (HEL) of the material.

The *x-t* data for the copper attenuation experiments is shown in Fig. 18, along with a dotted line representing the attenuation curve in PMMA. Note that *two* times are now given for each shock pin: one for the arrival of the elastic precursor and the other for the shock. Note also that contact gauges give times of arrival that significantly lag the shock pin signals, and this discrepancy increases as the shock decays. This suggests that contact gauges may not be appropriate for high impedance materials or materials with a large HEL.

The average shock speed in copper is faster than in PMMA, probably due to copper's higher initial sound speed and "c_0." This result should *not* necessarily be interpreted as a lower rate of shock attenuation in copper. In fact, Klee et al. [7] in trials similar the to

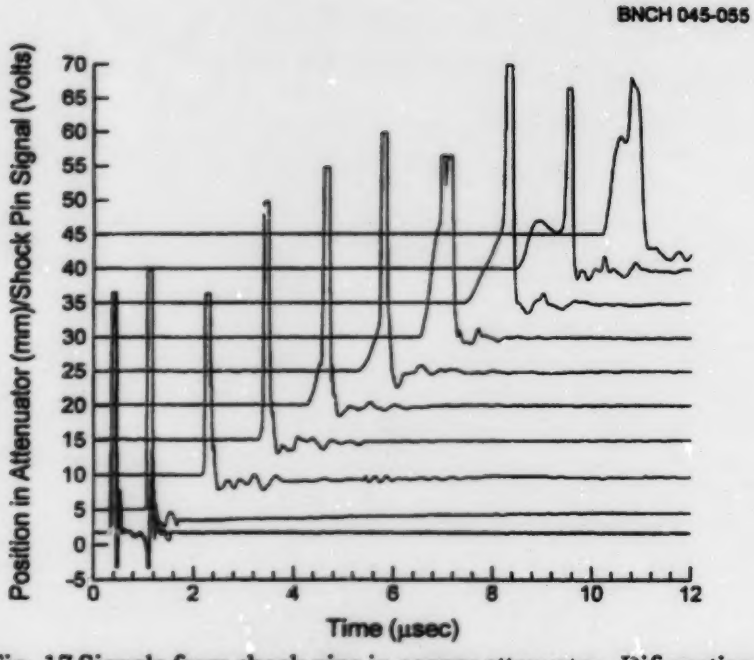

Fig. 17 Signals from shock pins in copper attenuator. Bifurcation of shock into elastic wave is visible.

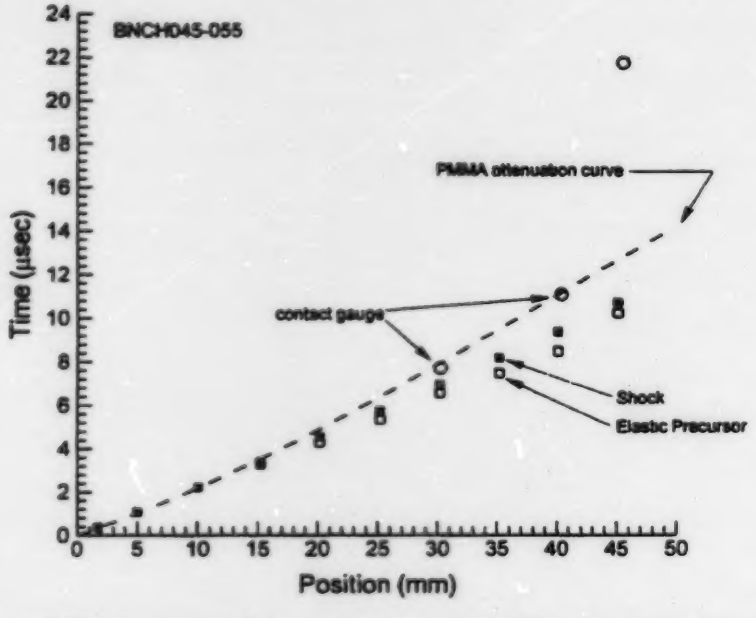

Fig. 18 Shock attenuation curve in copper (25 mm diameter) as compared to PMMA.

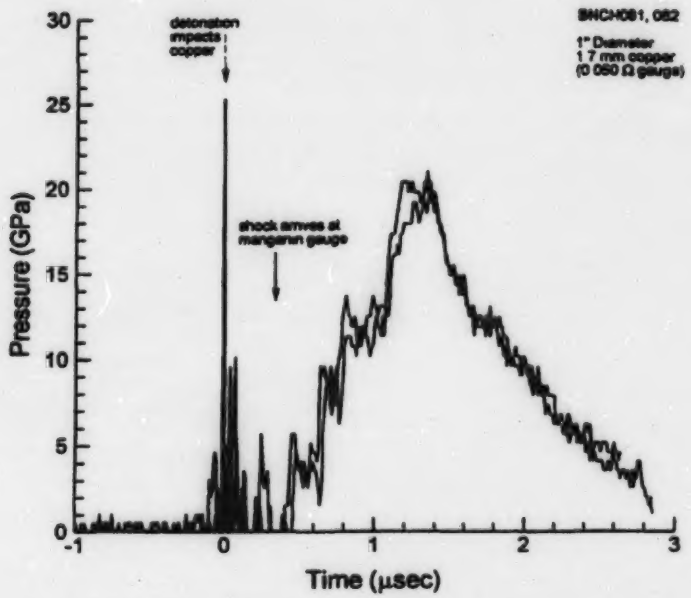

Fig. 19 Pressure profile in 25 mm copper attenuators (1.7 mm from explosive/copper interface) as measured by manganin gauges.

current experiments using RDX, HMX, TNT, and Tetryl as the donors, show that copper can have a higher attenuation rate than PMMA over most of the shock trajectory.

1.8.2 Manganin Gauge Measurements

Two experiments with manganin gauges embedded in a copper attenuator were attempted. The manganin gauge in both experiments was placed very close to the donor (1.7 mm). The signals returned from the gauges are shown in Fig. 19. Note that there is a large amount of noise prior to or coincident with the arrival of the shock. The manganin gauge did not show a distinct shock front, but rather a rise in a series of steps that took about 1 μs to reach a peak of 20 GPa, which agrees very well with the expected pressure of 20.7 GPa from impedance matching.[4] Note that bifurcation of the shock into an elastic precursor and plastic shock does not appear in the shock pin signals (Fig. 17) until 20 mm into the attenuator, and even then the peak is reached in much less than a 1 μs. Despite the good reproducibility of this experiment and correct amplitude of shock pressure, the manganin signal is regarded as suspect due to the large noise and slow rise of the signal. The fact that the attenuator is a conductor (copper) and was in direct contact with an electrical short (i.e., the TP located at $x = 0$) is a factor to consider in this experiment.

1.9 Summary of Attenuation Data

To summarize the results obtained with shock attenuation in PMMA that will be required to interpret the results in Part 2 of this report, the x-t trajectory of a shock in PMMA can be

Table 1: Summary of Curve Fits to Shock Attenuation in PMMA

$$t(x) = k_0 + k_1 t + k_2 t^2 + k_3 t^3$$

Curve Fit	x-range [mm]	k_0	k_1	k_2	k_3
25 mm global	0 - 45	1.1595×10^{-3}	1.8760×10^{-1}	3.2637×10^{-3}	-2.6705×10^{-5}
25 mm local	0 - 15	-1.5760×10^{-5}	1.8499×10^{-1}	3.3816×10^{-3}	-1.0640×10^{-5}
50 mm global	0 - 45	6.5950×10^{-3}	2.2197×10^{-1}	1.1323×10^{-4}	1.2897×10^{-5}
50 mm local	10 - 45	1.969×10^{-1}	2.1822×10^{-1}	-7.6185×10^{-4}	3.5276×10^{-5}

represented by the 3rd order curve fits summarized in Table 1, where the range of application of the curve fit is noted. Using the c_0, s Hugoniot for PMMA [5,6]:

$U_{shock} = c_0 + s\, u_{particle}$

Cooper [5]: $c_0 = 2.598$ km/s $s = 1.516$

Batsanov [6]: $c_0 = 2.510$ km/s $s = 1.545$ (valid $P = 5$-19 GPa)

the shock pressure at a given location can be approximated by:

$$P_{shock} = \rho_0 U_{shock} u_{particle}$$

The shock velocity is obtained directly from differentiation of the curve fit:

$$U_{shock} = 1/(dt/dx)$$

and the particle velocity is given by:

$$u_{particle} = (U_{shock} - c_0)/s$$

The density of PMMA is taken as $\rho_{PMMA} = 1.186$ g/cm^3. These "working relations" will be used in Part 2 below.

Part 2: Shock Initiation of Liquid Explosives

2.1 Introduction

Using the donor/attenuator developed and quantified in Part 1 of this report, the shock wave generated can now be used to study the shock initiation of nitromethane. This section (Part 2) discusses the experimental procedure and interpretation of diagnostics to determine initiation or failure to initiate. Results with both pure and sensitized nitromethane are presented with 25, 50, and 100 mm diameter charges.

2.2 Procedure

Experiments focusing on shock initiation of liquid explosives used the same donor/ attenuator configuration as described in Section 1.4. Now a "receptor" charge of test explosive is added under the attenuator, as shown in Fig. 20. The receptor is contained in a PVC capsule, usually of identical dimension to the donor (e.g. 25 mm diameter, 50 mm long). The bottom of the receptor is usually a glass plate, permitting visual inspection of the test charge and also optical access for photodiode/pyrometry measurements.

The test charge consisted of either pure Nitromethane (Aldrich commercial grade, 96% pure, Catalogue # 10, 817-0) or Nitromethane sensitized with 5% DETA by mass (99% pure, Aldrich Catalogue # D9, 385-6). If sensitized nitromethane was used, the mixture was prepared outside the capsule by mixing the appropriate mass fractions of NM and DETA. The two liquids were mixed shortly before the actual tests, usually within an hour. The sensitized charge was then poured into the test capsule. Any air bubbles visible in the test charge (e.g. adhering to the wall) were removed with a needle and syringe.

In order to prevent bubbles from being trapped at the attenuator/test explosive interface, the test charge was intentionally overfilled by using a "moat" of liquid explosive around the top of the test charge. The attenuator (already attached to donor as a single unit) could then be carefully lowered into the test explosive and then "snapped" into place without permitting air bubbles in. The bottom of the PMMA attenuator was usually covered with a layer of Parafilm (see Appendix A). This layer was pinched between the attenuator and the lip machined on the test capsule, ensuring a good seal.

After the donor/attenuator was snapped into place, the test charge was visually inspected and the presence of any bubbles noted. No special precautions were taken to prevent gas bubbles; the nitromethane was not degassed prior to testing. If a large bubble was introduced in the process of attaching the donor charge, the donor and attenuator were removed and the test charge refilled.

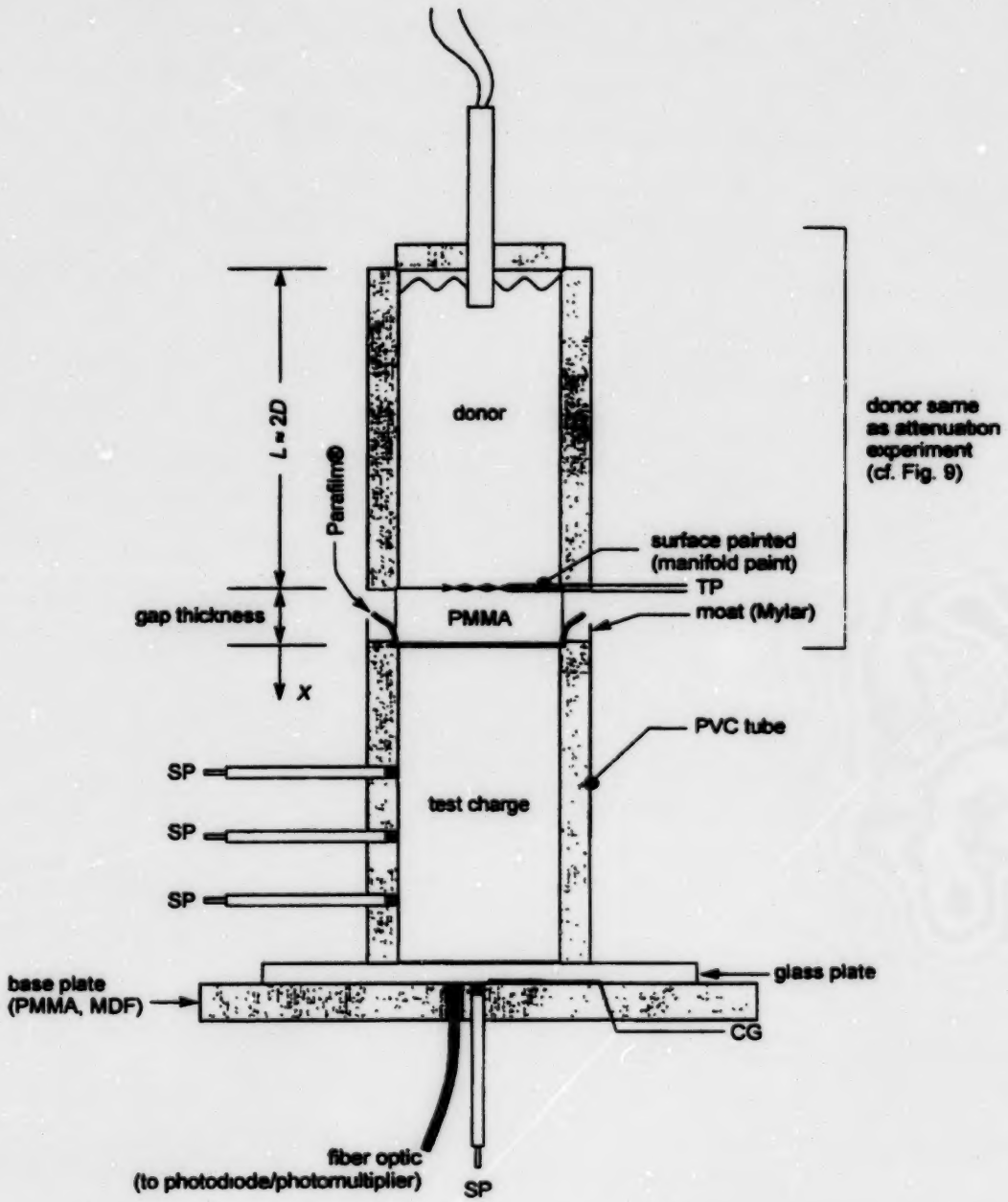

Fig. 20 Charge configuration for initiation experiments (25, 50, and 100 mm scale). Donor and test capsule identical to capsule used for attenuation experiments (cf. Fig. 9).

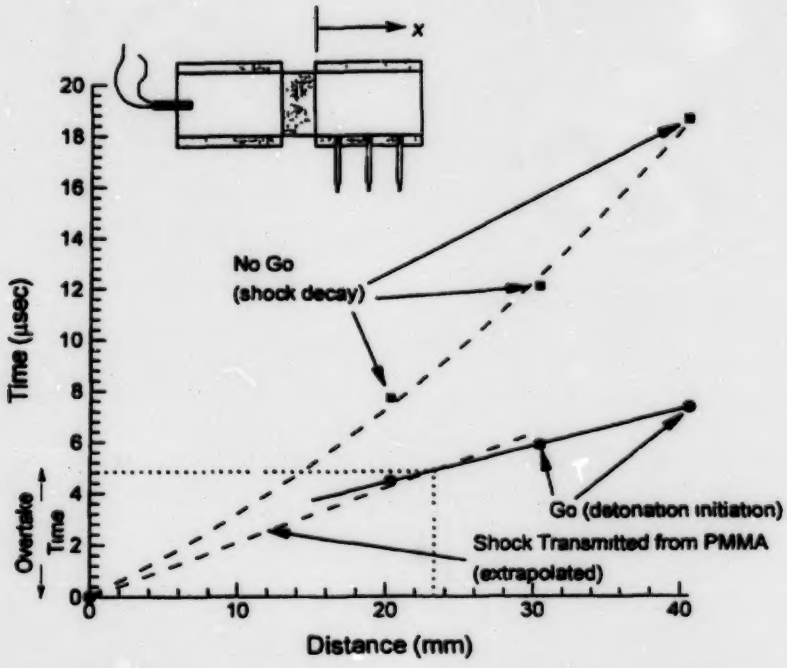

Fig. 21 Same results showing successful initiation ("Go") and failure of initiation ("No Go") of detonation in sensitized nitromethane.

2.3 Sample "Go" and "No Go" results

Figure 21 shows the two representative outcomes of these experiments: the case in which a detonation is formed ("Go") and the case where no detonation was initiated ("No Go"). The three shock pins located along the wall of the test charge give the time of arrival of the shock or detonation traveling along the test charge. The data points that appear on Fig. 21 were obtained with a 25 mm diameter test charge of NM + 5% DETA, using shock pins for shock time of arrival. The time of shock wave entry into the nitromethane (time zero) was not directly measured for initiation experiments. Instead, the shock *x-t* trajectory measures in Part 1 was used to estimate the transit time of the shock across the PMMA gap.

The "Go" result corresponds to an attenuator thickness of 5 mm, while the "No Go" result was from an experiment with a 10 mm thick attenuator. The result with the thicker attenuator clearly shows a decelerating shock (curve fit of shock trajectory shown as dashed line). The shock pin signals with the 5 mm attenuator show a wave propagating at a constant velocity of 6 km/s, which is clear evidence of a detonation propagating along the charge. Note, however, that extrapolating a line backward from these three points does not intersect the origin, where the shock entered the test charge. This result suggests that, in this experiment, there was a delay between the shock entrance and the initiation of

detonation. This is consistent with the current picture of shock initiation in homogeneous explosives: an inert shock enters the explosive and after a delay, a reaction front forms behind the shock in the compressed explosive. This reaction front propagates forward as a "superdetonation", eventually overtaking the initial shock.

While the results in Fig. 21 are consistent with planar shock initiation, they cannot be use to reliably measure a shock "overtake" distance (i.e., the distance required for the superdetonation to overtake the initial shock). Repeats of the "Go" experiment sometimes resulted in the back-extrapolation of the detonation arrival times giving a *negative* time of detonation initiation. This result is clearly nonphysical, and may result from the fact that shock pins mounted on the wall give only a one-dimensional measure of a multidimensional initiation process that could involve interaction with the capsule walls. Thus, until the details of the mechanism of initiation in this particular experiment are better understood, the results in Fig. 21 cannot be used as a source fundamental shock initiation data.

Finally, the possibility of Low Velocity Detonation (LVD) must be considered when the initiating shock interacts with the confinement of the test charge. LVD can occur with much lower shock input pressures than required for the initiation of high order detonation. LVD propagation speeds in nitromethane, however, are consistently reported at velocities of less than 2.5 km/s. Thus, while the occurrence of LVD cannot be completely ruled out of these experiments, if LVD occurs it would be interpreted and reported as a "No Go" result. The result of an experiment reported as a "Go" is definitely a high order detonation with a propagation velocity on the order of 6 km/s.

2.4 Results with Pure Nitromethane

Experiments performed with pure nitromethane (Aldrich commercial grade, 96% pure) as the test charge are shown in Fig. 22 (the donor charge is NM + 10% DETA). Note that two experiments performed with 25 mm diameter charges did not result in initiation of the test, even though a very thin attenuator was used (2 mm). At the 50 mm scale, four trials were conducted with a 2 mm thick PMMA attenuator. At this larger scale, inconsistent results were obtained: 2 of the 4 trials resulted in initiation. Increasing the attenuator thickness to 4 mm always resulted in two consistent "No Go" results. The 50% Go / 50% No-Go results obtained at the 50 mm scale suggest that 2 mm is near the critical gap thickness for this test configuration. Such a thin attenuator, however, makes it difficult to determine the sensitivity of initiation to various parameters.

On the basis of these results, no further experiments were conducted with pure nitromethane. As discussed in Section 2.4 below, initiation in pure nitromethane would likely require much larger diameter charges and a stronger initiating shock (and hence more powerful donor than nitromethane). At this point, the decision was made to pursue further tests only using sensitized nitromethane as the test explosive. Being more shock sensitive, nitromethane sensitized with DETA will have a thicker critical thickness of PMMA, permitting the dependence of attenuator thickness (and thus shock sensitivity) to more readily be determined as a function of other experimental parameters.

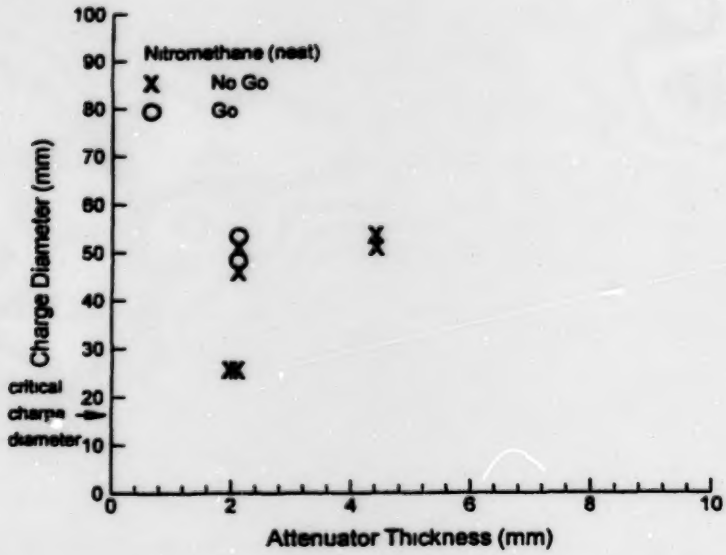

Fig. 22 Summary of results with pure (unsensitized) nitromethane.

2.5 Results with Sensitized Nitromethane

While there exists a large body of data in the literature on shock initiation of explosives for pure nitromethane, comparatively little data exists on sensitized nitromethane.[8] report measurements of shock overtake distance and time for nitromethane sensitized with 5% DETA. James et al. [9] and Cook et al. [10] report on experiments with shock initiation NM + 5% DETA by cylindrical projectile. In order to permit quantitative comparison of the current experiments to this prior data, nitromethane sensitized with 5% DETA was used here as well.

2.5.1 Results at 25 mm Scale

Results with donor and test charges of 25 mm in diameter are summarized in Fig. 23, showing the thickness of PMMA attenuator and the outcome of the experiment, as determined by shock pins or contact gauges mounted on the test charge, either "Go" or "No Go." Note that some data points are shifted up and down in order to permit easy viewing; all the experiments had the same diameter charge (25 mm). The critical thickness of PMMA attenuator is in the range of 8 to 10 mm. Attenuators thinner than 8 mm always resulted in initiation; attenuators thicker than 10 mm were never able to initiate the donor charge. From Fig. 16, this corresponds to a shock pressure in the PMMA of 6.8 GPa and 5.6 GPa, for 8 and 10 mm thick attenuators, respectively. From impedance matching calculations [4], the pressure of the shock transmitted into the nitromethane test charge can be estimated to be between 5 and 6 GPa. Thus, this would be the critical shock pressure for this charge configuration.

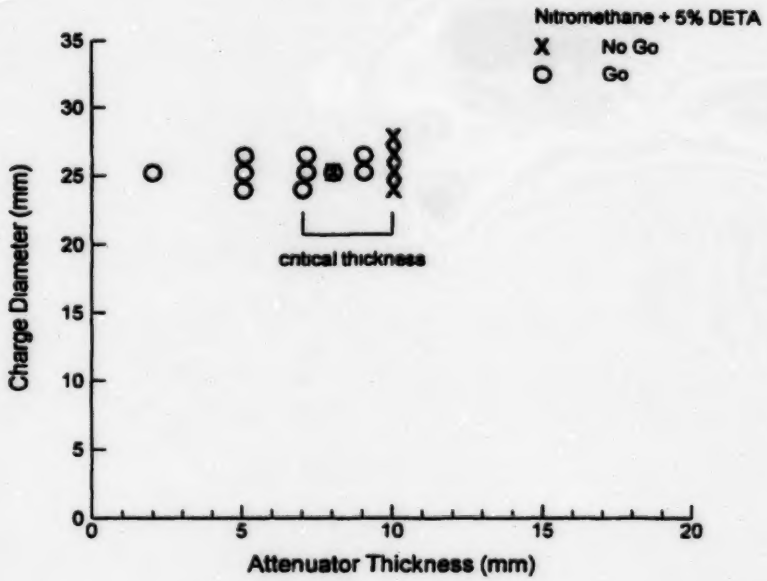

Fig. 23 Summary of results with sensitized nitromethane at 25 mm scale.

Note that, with the exception of a single "No Go" result at 8 mm, the experiments in Fig. 23 have excellent reproducibility. This is typical of gap tests, and should *not* necessarily be taken as evidence that the current results are "ideal" planar shock initiation experiments.

2.5.2 Results with Longer Donor (25 mm Diameter)

In order to determine the factors responsible for failure of initiation to occur with attenuators thicker than the critical value, the 25 mm diameter experiment was repeated with a donor charge 6" long, rather than 2" long (as shown in Fig. 24). This three-fold increase in the length of the donor should result in reduced gradient in the Taylor wave following the detonation. If rear-generated longitudinal rarefactions are a factor in initiation, then this may affect the results of an experiment. Fig. 25 shows, however, that failure of initiation still results if a 6" long charge is used instead. This implies that *lateral*, rather than longitudinal, rarefactions cause failure of initiation in the sub-critical experiments.

2.5.3 Results at Larger Scale

Results of experiments investigating shock initiation of sensitized NM with larger diameter charges (50 mm and 100 mm, as shown in Fig. 26) are shown in Fig. 27, along with the prior results with 25 mm diameter charges. Due to the expense of field trials using large diameter experiments, only 5 experiments were performed at the 50 mm scale and 6 experiments at the 100 mm scale. Thus, there exists a relatively large uncertainty in

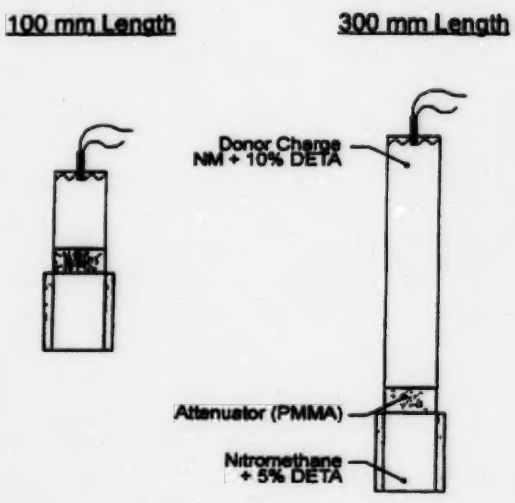

Fig. 24 Schematic of charges used to investigate the effect of donor length on shock initiation.

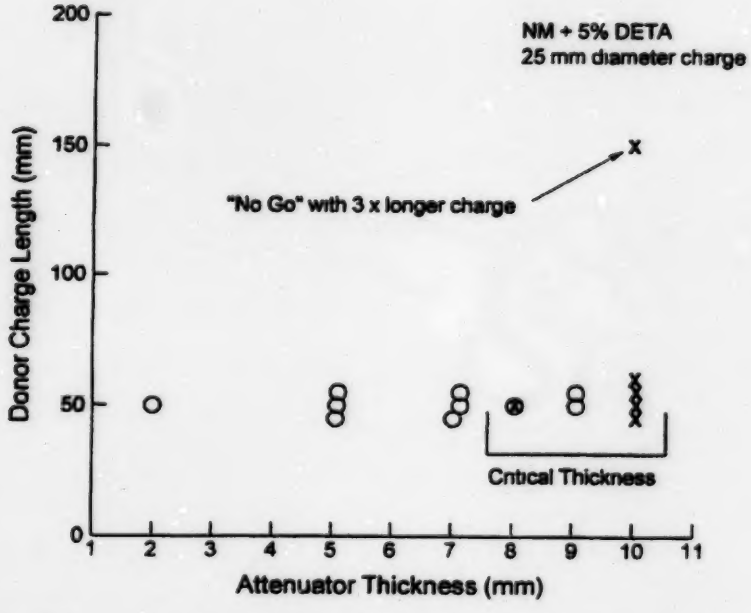

Fig. 25 Summary of results with sensitized nitromethane at 25 mm scale with longer donor charge.

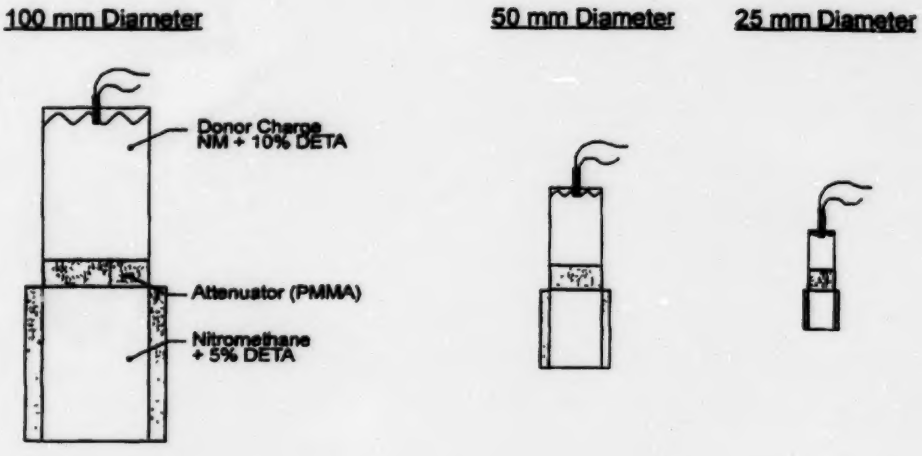

Fig. 26 Schematic of charges used to investigate the effect of diameter on shock initiation.

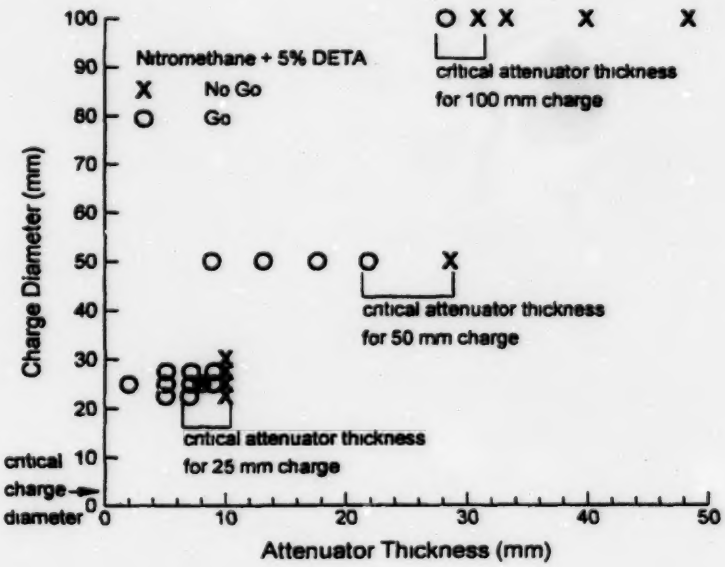

Fig. 27 Summary of results with sensitized nitromethane with variable diameter charges.

Table 2: Summary of Experiments with Sensitized Nitromethane

Charge Diameter [mm]	Critical Result	PMMA Thickness [mm]	PMMA Shock Pressure (cf. Fig. 16) [GPa]	Nitromethane Shock Pressure [4] [GPa]
25	Go	8	5.5	4.9
	No Go	9	5.0	4.4
50	Go	22	4.9	4.3
	No Go	29	3.8	3.3
100	Go	28	4.0	3.5
	No Go	31	3.6	3.2

the critical thickness of PMMA gap as compared to the experiments at the 25 mm scale. Despite these large error bars, the experiments at 50 mm clearly have a much greater critical gap thickness (PMMA gap: 22-29 mm) as compared to the results at 25 mm (PMMA gap: 8-10 mm). The results at 100 mm also appear to have a greater critical gap thickness than at 50 mm, although the data sets only overlap at one point (28-29 mm), where the 50 mm experiment was a "No Go" and the 100 mm experiment was a "Go." Thus, it is unclear if the results have asymptoted to constant gap thickness when the charge diameter reaches 100 mm.

Also indicated in Fig. 27 is the critical charge diameter of weakly-confined NM + 5% DETA, given by Lee et al. as approximately 3 mm.[11] Note that this charge diameter is at least one order of magnitude smaller than the charges used in these experiments.

The results of the experiments with different diameter charges is summarized in Table 2, along with the shock pressure in the PMMA at the critical thickness (as given by Fig. 16) and the transmitted shock pressure in nitromethane, as predicted by impedance matching calculations.[4]

2.6 Analysis

The results reported here clearly indicated that it is the diameter of the charge, rather than the length of the donor, that dominate the ability of a shock to initiate a charge of sensitized nitromethane. Even as this diameter is made more than an order of magnitude greater than the critical diameter of the unconfined explosive, the results of a shock initiation experiment are still dependent on the diameter of the charge. Possible explanations of this dependence are explored below.

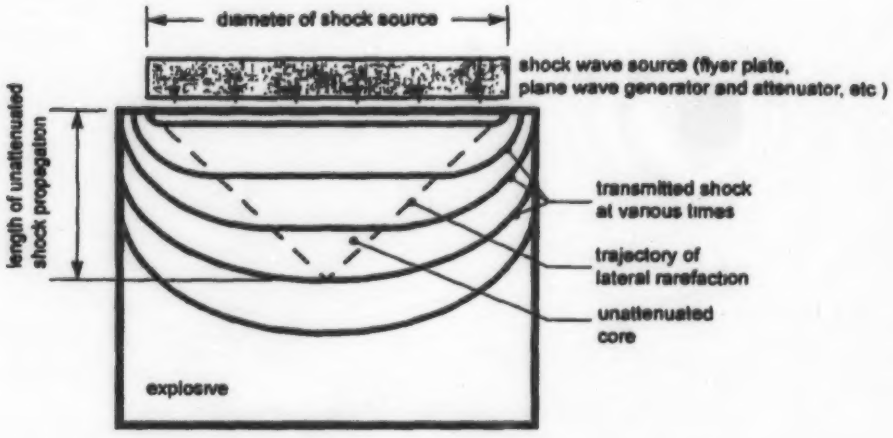
diameter of shock source
shock wave source (flyer plate, plane wave generator and attenuator, etc)
length of unattenuated shock propagation
transmitted shock at various times
trajectory of lateral rarefaction
unattenuated core
explosive

Fig. 28 Sketch showing the attenuation of a transmitted shock due to lateral rarefactions.

2.6.1 Interpretation

A possible explanation for the effect of scale on the shock initiation of nitromethane in these experiments can be considered from Fig. 28. In this figure, a shock wave is transmitted into the test explosive by planar shock source (e.g., a flyer plate or planar wave generator). As the shock propagates into the explosive, the effect of the finite size of the charge is propagated inward by rarefaction waves. These rarefaction waves lower the pressure and temperature of the explosive, lowering the reaction rates and possibly quenching reaction altogether. If these rarefactions reach the center before detonation has been initiated, then they may prevent the initiation of detonation, even if the initial shock was strong enough to initiate detonation in a larger (effectively semi-infinite) charge.

For a material with a known c_0, s Hugoniot, the speed of the inward propagating rarefactions can be approximated by [5]:

$$c_{\text{rarefaction}} = c_0 + 2s\, u_{\text{particle}}$$

For most materials and at the range of shock pressures of interest, this speed is very close to the shock speed itself. Thus, the rarefactions propagate inward along a trajectory of 45° relative to the direction of shock propagation. This provides a simple geometric criterion for the effect of scale on shock initiation: the radius of the charge should be greater than the ideal shock-to-detonation transition distance.

This criterion is dramatically validated by the data of Moulard and Wenograd for detonation initiation in Composition B by cylindrical free-flying impactors. As shown in Fig. 29 (reproduced from Cooper [5]) there is remarkably good agreement between the critical diameter of the impactor and the ideal run-up distance for the same shock pressure obtained from the so-called "Pop-plot."

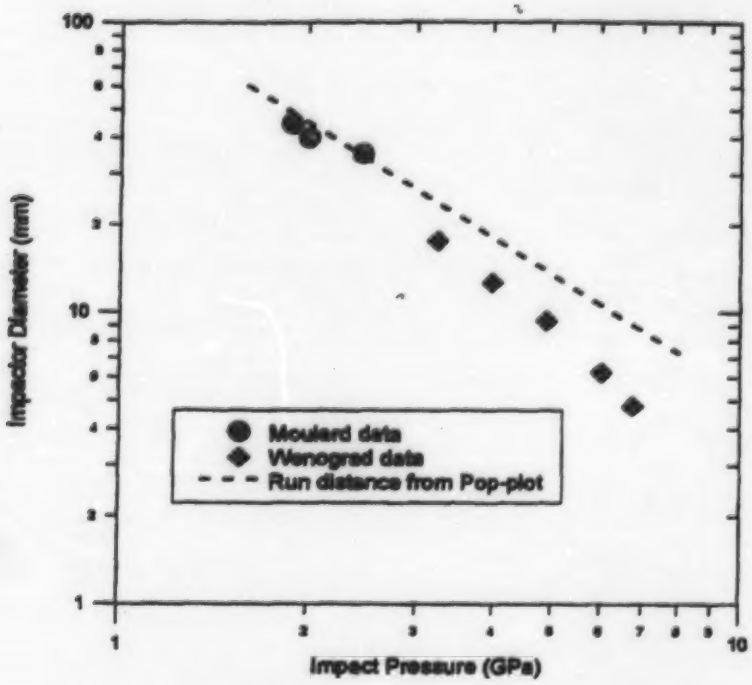

Fig. 29 Plot showing the effect of shock generator diameter (flying plate, in this case) on shock initiation. Taken from [5].

Although the current experiments do not transmit an initially planar, constant-amplitude shock as in the case of an impactor, due to the point initiation of the donor and the fact that lateral rarefactions have already propagated into the attenuator before the shock has entered the nitromethane, this geometric criterion provides a possible explanation for the effect of charge diameter. In order to provide a quantitative comparison, similar to Fig. 29 for the Moulard and Wenograd, data on the ideal shock overtake distance is required.

2.6.2 Comparison to Published Data on Sensitized Nitromethane

The only data available on the ideal shock initiation of nitromethane sensitized with 5% DETA are the gas gun experiments of Sheffield et al.[8] These experiments used a precision impactor to transmit a shock into a nitromethane charge contained in a 70 mm diameter PMMA capsule containing sensitized nitromethane. The results of an experiment were determined using Lagrangian gauges imbedded in the liquid charge. This technique permitted direct observation of the build up of a reactive wave in the shock compressed material and its coalescence into a suspected superdetonation. Only two experiments are reported, and in only one did the superdetonation overtake the shock within the region monitored with gauges, permitting the overtake distance to be directly measured. These values are reproduced in Table 3, with the overtake distance of 7.8 mm being an extrapolation rather than a direct measurement. Sheffield et al. observed that the

Table 3: Shock Initiation of Sensitized Nitromethane, Sheffield et al.[8]

Calculated Shock Pressure [GPa]	Measured Shock Pressure [GPa]	Shock Overtake Distance [mm]	Shock Overtake Time [μs]
6.8	6.2	3.3	0.9
5.8	5.1 - 5.5	7.8*	2.0

*Extrapolated, not directly measured.

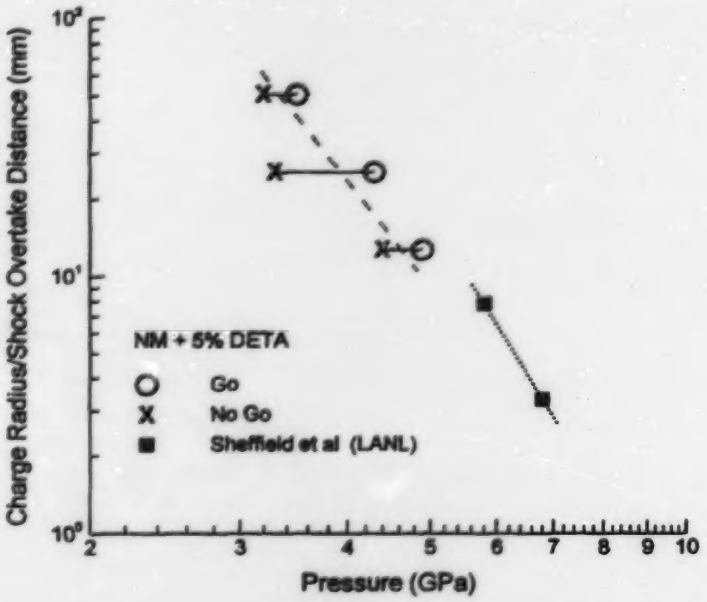

Fig. 30 Comparison of current results with the planar shock initiation experiments of Sheffield et al.[8]

actual pressure behind the incident shock (as measured by the Lagrangian gauges) was about 10% lower than impedance matching calculations would predict, suggesting the possibility of chemical reaction affecting the "nonreacting" incident shock wave. The values used above, however, are the *predicted*, not measured, values, to provide a consistent comparison to the current data. Sheffield et al. also noted that their experiments are not purely homogeneous experiments due to the presence of salts in suspension in NM sensitized with large amounts of DETA (which are also present in the current experiments) and also due to the presence of the Lagrangian gauges themselves (which are not present in the current experiments). These possible disturbances have an unknown effect on the experiment.

In Fig. 30, the "ideal" shock overtake data of Sheffield et al. is compared to the current data. This figure plots the shock overtake distance as a function of pressure for the

Table 4: Projectile Initiation of Sensitized Nitromethane, Cook et al.[10]

Projectile Diameter [mm]	Critical Velocity [m/s]	Shock Pressure in NM (steel impact) [GPa]	Shock Pressure in Al (steel impact) [GPa]	Shock Pressure in NM (transmitted from Al) [GPa]
8.0	1533	6.04	20.0	7.99
13.15	1338	4.93	17.0	6.57
20.0	1122	3.82	13.9	5.13

Sheffield data, and the charge radius versus the critical shock pressure for the current gap test results. Note the large band of uncertainty in the critical shock pressure for the present results, especially at the 50 mm scale. The two data sets appear to overlap with similar slopes.

The experimental results most similar to the current experiments available in the literature are the projectile initiation trials of Cook et al.[10] In their experiments, flat-ended steel cylinders were fired into capsules of nitromethane contained in PMMA cylinders. The flat end of the capsules though which the projectile impacted was sealed with an aluminum plate. The exact thickness of this plate is not given, but based on an earlier publication [9] in which the plate thickness was varied from 1 to 8 mm, the thickness used for these particular trials was 1 mm. The projectile diameter varied from 8 to 20 mm. This was smaller than the 57 mm diameter of the charge. Experiments were performed with pure nitromethane, nitromethane sensitized with 5% DETA, and nitromethane gelled with 7% polyethylene oxide and then sensitized with 1% glass microballoons. The results of the firings were determined by direct observation with an Imacon 468 camera. The critical velocity for initiation is shown for the different projectile diameters in Table 4. The shock pressure of the aluminum plate resulting from the impact of the steel projectile, and the shock pressure of the nitromethane resulting from the shock transmitted through the aluminum plate are also listed in the table. This pressure applies only during the initial stages of shock transmission into the nitromethane. As rarefaction waves propagate back and forth in the relatively thin aluminum plate, the shock pressure should approach the value of direct steel impact on nitromethane (as listed in Table 4), which is about 25% lower than the pressure obtained initially from the aluminum plate.

The Cook et al. experiment can be directly compared to the current results. The projectile radius corresponds to the donor charge radius. If the initial shock pressure for the critical projectile velocity is compared with the current results, the agreement is satisfactory, as shown in Fig. 31. Note that the impedance matching calculations based off the shocked state of the *aluminum* is used, rather than the impact of steel, since this is the initial pressure. Likewise, in the current gap test experiments, the initial peak transmitted shock pressure is used, even though the pressure decays behind the shock and the peak shock pressure itself decays as it propagates into the test charge. In both cases, the actual shock

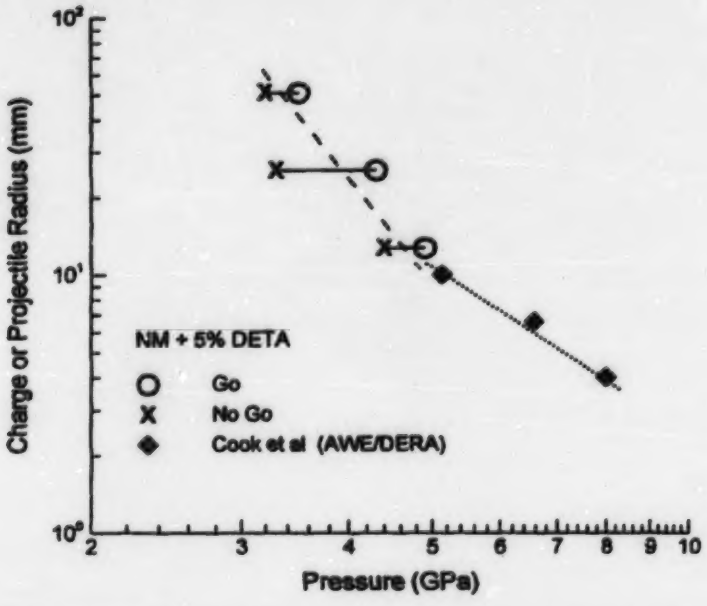

Fig. 31 Comparison of current results with the projectile impact initiation experiments of Cook et al.[10]

pressure over the duration of the initial event is less than the value used in Fig. 31, making more quantitative comparisons of these experiments difficult.

2.7 Conclusions

While the results of shock initiation experiments presented in this report cannot be considered as a source of fundamental data on shock initiation, due to a variety of factors (nonplanar shock, interaction with confinement, etc.), the results do appear consistent with the established picture of initiation of homogenous liquid explosives. Quantitative comparisons with the "ideal" shock initiation experiments of Sheffield et al. [8] and the projectile impact trials of Cook et al. [10] show that the current gap experiments are at least consistent with the limited available data on shock initiation of nitromethane sensitized with DETA. It appears that the lateral rarefactions generated by the finite diameter of the charge are the dominant factor in determining if initiation will occur for a given level of shock loading. The general criteria that the shock generator should have a radius greater than the ideal shock overtake distance for initiation to occur seems valid for these experiments.

The major unresolved issue in the present results is the role of the confinement of the test charge. The transmitted shock interacts with the PVC walls of the test capsule, which has a higher shock impedance than the nitromethane itself, possibly resulting in shock reflections, precursor shocks, and other non-ideal effects that can significantly affect the results in comparison to an "ideal" unconfined (or effectively semi-infinite) charge (see

Appendix C for impedance matching calculations of nitromethane vs. capsule material). These questions will only be resolve with further advances in diagnostics that can spatially and temporally resolve the mechanism of initiation, rather than just the "Go" or "No Go" nature of the current experiments.

Acknowledgements

The work described in this report was performed by François-Xavier Jetté and Akio Yoshinaka. Massimiliano Romano was responsible for the electronics and instrumentation. Samuel Goroshin and David Frost (McGill University) are recognized for their assistance and advice. Richard Bowes (CANMET) is thanked for use of the CERL blast chamber, and the technical staff of DRES is acknowledged for their support in the field trials.

References

1. Suceska, M., *Test Methods for Explosives*, Springer-Verlag, New York, p. 45 (1995).
2. Campbell, A. W., Davis, W. C., and Travis, J. R., "Shock Initiation of Detonation in Liquid Explosives," *Phys. of Fluids*, 4, no. 4, p. 498 (1961).
3. Walker, F. E., Wasley, R. J., "Initiation of Nitromethane with Relatively Long-Duration, Low-Amplitude Shock Waves," *Combust. Flame*, 15, p. 233 (1970).
4. Mader, C.L., *Numerical Modeling of Explosives and Propellants*, 2nd ed., CRC Press, New York (1998).
5. Cooper, P., *Explosives Engineering*, Wiley-VCH, New York (1996).
6. Batsanov, S.S., *Effects of Explosions on Materials*, Springer Verlag, New York (1994).
7. Klee, C., Kroh, M., Ludwig, D., "Experiments on the Attenuation of Shock Waves in Condensed Matter," Topical Conference on Shock Waves in Condensed Matter, *American Institute of Physics Conference Proceedings*, No. 78, pp. 486-490 (1981).
8. Sheffield, S.A, Engelke, R., and Alcon, R.R., "In-Situ Study of the Chemically Driven Flow Fields in Initiating Homogeneous and Heterogeneous Nitromethane Explosives," *Ninth Symposium (International) on Detonation*, Portland, OR, pp. 39-49 (1989).
9. James, H.R., Cook., M.D., Haskins, P.J., "The Response of Homogenous Explosives to Projectile Attack," *11th International Detonation Symposium*, Snowmass Village, CO (1998).
10. Cook, M.D., Haskins, P.J., Briggs, R.I., Cheese, P., Stennett, C., Fellows, J., "High Speed Observations of Fragment Impact Initiation of Nitromethane Charges," *Shock Compression of Condensed Matter*, ed. Furnish, M.D., Chhabildas, L.C., Hixson, R.S., American Institute of Physics, pp. 793-796 (2000).
11. Lee, J.J., Jiang, J., Choong, K.H., Lee, J.H.S., "Effect of Diethylenetriamine and triethylamine Sensitization on the Critical Diameter of Nitromethane," *Shock Compression of Condensed Matter*, ed. Furnish, M.D., Chhabildas, L.C., Hixson, R.S., American Institute of Physics, pp. 797-800 (2000).

Appendix A: Compatibility Tests with Nitromethane and DETA

Compatibility Tests with Nitromethane and DETA

Introduction

Nitromethane (NM) sensitized with 10% diethylenetriamine (DETA) was chosen as the donor explosive in the creation of a standard benchmark experiment. At the time of this report, two shock attenuating materials were being tested, namely, clear acrylic (polymethylmethacrylate or PMMA) and copper (99.9% pure). Furthermore, both donor and test charges are contained in capsules comprised of PVC, aluminum, glass and various sealants and epoxies. It has come to our attention that certain materials are incompatible with nitromethane and DETA. For example, as nitromethane dissolves PMMA, contact between the two will produce a "gummy and sticky" attenuator surface. This "softening" may result in potential donor charge leakage, in a change of mechanical (and perhaps Hugoniot) properties and could also affect the properties of the NM + DETA charge. Protection against interfacial chemical reactions between the shock attenuator and NM+DETA explosive was therefore investigated.

Protection of PMMA

PMMA was chosen as a benchmark material because of its low cost, availability, ease to machine but most importantly, its shock Hugoniot characteristics have been studied extensively.

Various chemical coating agents were tested for their ability to protect PMMA against NM and mixture of NM with DETA, namely:

1- Motormaster's "Exact Match" automotive paint
2- Motomaster's "High Heat Manifold Paint"
3- Motomaster's "Primer"
4- Motomaster's "Chrome Bumper Paint"
5- Flecto's "Varathane Professional Clear Finish"
6- Tremclad's "High Heat Enamel"
7- "Leak Sealer"
8- Mar-Hyde's "Vinyl Color"
9- Devcon's "5 min epoxy"
10- Pebeo's "Drawing Gum Liquid Frisquet"
11- Dow Corning's "732 Multi-Purpose Sealant"
12- M.G. Chemicals' "Silicone Resin Clear Lacquer"

13- Lepage's "BondFast White Glue"

14- Elmer's "Glue All"

15- Paraffin

16- Motomaster's "Primer for Flexible Auto Parts"

17- Motomaster's "Clear-coat"

18- Motomaster's "Engine Finish"

Compatibility is based solely on visual observation (whether the explosive mixture penetrates through or reacts with the coating agent). Following is a table of these coating agents and the results of their compatibility tests.

Product	Manufacturer	Coating type	Listed content(s)	Compatible with NM + 10%DETA	Comments
Exact Match	Motormaster	Automotive paint	Toluene	No	❑ Reacted a few minutes upon contact
Primer (flat gray)	Motormaster	Automotive primer	Acetone	No	❑ Coating agent peels off within an hour of exposure (i.e., dissolved) ❑ stains on surface
Chrome Bumper Paint	Motormaster	Chrome bumper paint	Toluene and Mineral spirits	Average	❑ Coating non-uniform (some spots present, probably due to long residence time on shelf) ❑ Stains on surface after exposure
High Heat Manifold Paint (aluminum color)	Motormaster	High heat manifold paint	Petroleum distillate and Acetone OR Toluene	Average	❑ Requires 2 coats (2nd applied immediately after 1st one) ❑ Few PMMA samples coated with it were left with faint stain after approximately 1 hr ❑ Exposure exceeding 24 hrs results in mixture penetrating surface
Varathane Professional Clear Finish	Flecto	Spray Varnish (900 clear gloss)		No	❑ Washed away upon contact
Leak Sealer	Leak Sealer	White spray to seal cracks in all types of surfaces		No	❑ Coating agent peels off within an hour of exposure
Paraffin		Paraffin (white wax bought in grocery stores)	Paraffin	Yes	❑ Coating appears inert to NM+DETA mixture

Product	Manufacturer	Coating type	Listed content(s)	Compatible with NM + 10%DETA	Comments
High Heat Enamel (flat black)	Tremclad	High heat enamel (e.g., for barbecues)	Petroleum distillates	Average	❑ Peels off 3hr45mins after exposure
Vinyl color (gloss black)	Mar-Hyde	Vinyl colored paint for touch-ups or color changes to vinyl and leather (e.g., for car seats)	Methyl Ethyl Ketone, Isobutyl Acetate and Toluene	No	❑ Appearance of stains and softening of coating
732 Multi-Purpose Sealant	Dow Corning	RTV sealant (100% silicone rubber)	Silicone rubber with acetic acid carrier	Yes	❑ Coating appears inert to NM+DETA mixture
Drawing Gum Liquid Frisquet	Pébéo	Drawing gum liquid frisquet	Water based	Average	❑ Soluble in water when still wet ❑ Light blue liquid ❑ Blue translucent when dry ❑ Forms a flexible, rubber-like film ❑ NM+DETA penetrates coating after exposure in excess of 10 hrs
Silicone Resin Clear Lacquer	M.G. Chemicals	Protective coating for PC boards		No	❑ Washed away on contact
Bondfast White Glue	Lepage	White glue		No	❑ Becomes gelatinous within hours of exposure to NM ❑ Becomes white like its original color ❑ Glue lifted from surface ❑ Exposure lasted 70 hrs ❑ Strong solvent smell emanating

Product	Manufacturer	Coating type	Listed content(s)	Compatible with NM + 10%DETA	Comments
Glue All	Elmer	White glue		No	❑ Same comments as for Bondfast White Glue
5 min Epoxy	Devcon	5 min Epoxy		No	❑ Becomes soft after exposure lasting 2hrs and 20 mins. ❑ Pure NM becomes yellow
Engine Finish (clear color)	Motomaster	Clear heat resistant engine finish	Acetone and Toluene	No	❑ Surface becomes gelatinous and sticky after 10 minutes ❑ Requires 2 coats (2nd applied immediately after 1st one)
Clear-coat	Motomaster	Protective and enhancing coating for car basecoat finishes	Acetone and Toluene	No	❑ Dissolved almost immediately ❑ Surface becomes deformed and bubbles appear under it ❑ Requires 2 coats (2nd applied immediately after 1st one)
Primer for flexible auto parts (clear color)	Motomaster	Primer for flexible auto parts	Toluene	No	❑ Surface softens a little and becomes sticky after 10 minutes ❑ Requires 2 coats (2nd applied immediately after 1st one)

Donor charge container material

In order to choose a material for the donor charge container, various plastics were also tested for compatibility with NM or mixtures of NM with DETA, namely,

1- Lexan
2- PolyMethylMethAcrylate (PMMA)
3- PolyPropylene (PP)
4- ABS
5- Clear PolyVinyl Chloride (clear PVC)
6- Gray PolyVinyl Chloride (gray PVC)
7- PETE
8- PolyStyrene (PS)
9- CPVC
10- Parafilm
11- Teflon

Compatibility is based solely on visual observation (whether the NM or DETA penetrates through or reacts with the plastic material). Following is a table of these materials and the results of their compatibility tests.

Product	Color	Compatible with NM + 10% DETA	Compatible with DETA	Compatible with NM	Comments
Lexan	Translucent			No	❑ Flakes and cracks once dried ❑ Deforms and dissolves under NM exposure
PMMA	Clear			No	❑ Surface becomes gelatinous almost immediately
Polypropylene	Cloudy White			Yes	❑ Appears inert to NM
ABS	Black			No	❑ Dissolves immediately (i.e., few minutes) upon contact with NM
Clear PVC	Clear			Average	❑ Becomes white and opaque after a few minutes ❑ Softens when in contact with NM ❑ Once "dry", stiffer than if unexposed to NM ❑ NM becomes slightly yellow
Gray PVC	Gray	Average		Average	❑ Starts to soften very slightly after very long exposure to NM (i.e., 13 days) ❑ PVC slightly "swells" ❑ NM becomes a little dark
PETE	Clear			Average	❑ Used a Naya™ spring water bottle; becomes white and opaque in some areas of the bottle ❑ Increases in thickness by 0.003" after 30 days in NM

Product	Color	Compatible with NM + 10% DETA	Compatible with DETA	Compatible with NM	Comments
Polystyrene	Clear			Average	❑ Increased in thickness from 0.119" to 0 124" when exposed to NM for 6 days minus 6 hours (evidence of slight surface reaction) ❑ Slight distortion in transmitted light ❑ No noticeable changes when exposed to denatured alcohol for 6 days
CPVC	Pale beige	No	No	Average	❑ Turns brownish, soft and sticky after a few minutes in DETA
Parafilm	Translucent		Average	Yes	❑ Was used to protect the top surface of an acrylic disc and to seal from NM ❑ After nearly a month the disc remained protected ❑ Exposed to pure DETA for 22 days; become yellowish after 40 minutes of exposure to DETA; it was clear again 8 days later. After removal from DETA, was rinsed with water and alcohol ❑ Looses its elasticity in certain localized regions
Teflon	White	Yes		Yes	❑ Appears inert to NM and mixtures of NM and DETA

Appendix B: Photodiode Circuit

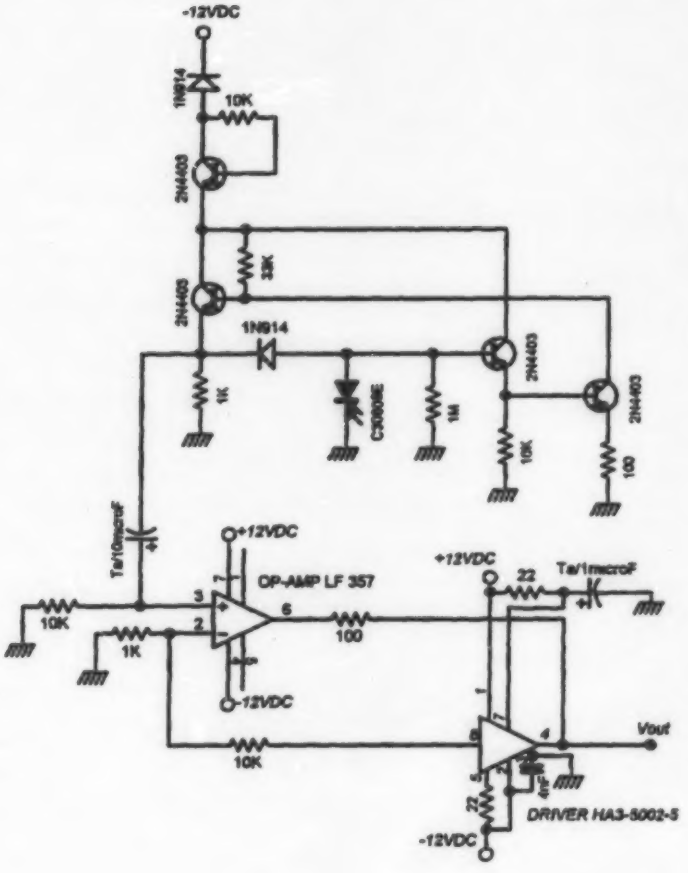

Appendix C: Impedance Matching Calculations of Various Materials

Impedance Matching Calculations of Various Materials

A short routine has been programmed in Matlab to calculate the state at the interface of two materials when a shock transmits from one to the other. This was done keeping in mind the charge setup for shock initiation experiments. Assuming a given shock strength emerging from the attenuator (PMMA for instance), what is the shocked state in the test liquid (NM for instance) after shock transmission from the attenuator? The code was originally designed to perform this calculation and graph the interaction on a *P-u* diagram. One assumption is made in this code: the left going Hugoniot is an exact mirror image of the right going Hugoniot.

This program is able to handle any material as the attenuator and any material as the test liquid provided the $U = C + Su$ equation (the *U-u* Hugoniot) is known for these materials (the *U-u* Hugoniots used in the code were obtained from the LASL Shock Hugoniot Data). The code was later modified to calculate independently the shocked state in two different materials for the same attenuator shock pressure. This new feature allows the calculation of the shocked state in the test liquid and its container when a shock transmits from the attenuator to both of them simultaneously. The data produced therewith permits an estimate of whether the transmitted shock in the container is faster than that transmitted in the test liquid (i.e., whether we will observe a precursor shock in the liquid). It also permits determination of whether a rarefaction or a shock will transmit from the container to the test liquid once both are shocked.

A few of the runs done with the materials of interest for this report are reproduced here. Typically, the attenuator is PMMA and the liquid is nitromethane. In the table, for each set of attenuator/liquid/container material arrangement, the code was run twice: once for a 2 GPa shock emerging from the attenuator (referred to as case 1 in the table), and once for a 10 GPa shock (referred to as case 2). In each case, the shock velocity and the shock pressure were calculated in both the liquid and the container.

Shock transmission is from attenuator to liquid and container

Attenuator	Liquid	Container	Shock velocity 1*		Interface pressure 1		Shock velocity 2		Interface Pressure 2	
			liq.	cont.	liq.	cont.	liq.	cont.	liq.	cont.
PMMA	NM	Teflon	2.7677	2.5719	1.7399	2 3708	4.4491	4.2053	8 9225	12 5401
PMMA	NM	PVC	2.7677	3 0357	1.7399	2.05	4.4491	4 68	8.9225	10.3754
PMMA	NM	2024 Aluminum	2.7677	5.6269	1.7399	3.501	4.4491	6.5896	8 9224	17.3053
PMMA	NM	6061-T6 Al	2.7677	5.6551	1.74	3.476	4 4491	6.6326	8.9225	17.1411
PMMA	NM	Polyethylene	2 7677	3.6988	1.7399	1.8232	4.4491	5.5242	8.9225	8.9528
PMMA	NM	Polystyrene	2.7677	3.4391	1.7399	1.8865	4.4491	5.0463	8.9225	9.188
PMMA	NM	Nylon	2.7677	3.4979	1.7399	2.001	4.4491	5 5669	8.9225	10.2861
PMMA	NM	Polyurethane	2.7677	3 2649	1.7399	2.0398	4.4491	5 0377	8.9225	10.3113
PMMA	NM	Polypropylene	2.7677	3.6492	1.7399	1.796	4 4491	5 4525	8 9225	8 8116
PMMA	NM	Lead	2 7677	2 2553	1.7399	3.9227	4.4491	2.9554	8 9225	21.1095
PMMA	NM	Rubber	2.7677	2.5989	1.7399	1 879	4.4491	4.254	8.9225	9.784
PMMA	Water	Polypropylene	2 7684	3 6492	1 6127	1 796	5 0525	5 4525	8.9392	8.8116
PMMA	Water	Teflon	2.7684	2 5719	1.6127	2.3708	5.0525	4 2053	8.9392	12.5401
PMMA	Water	Polyethylene	2.7684	3.6988	1 6127	1.8232	5.0525	5.5242	8.9392	8.9528
PMMA	Water	Polystyrene								
PMMA	Ethyl Alcohol	Teflon	2.7314	2 5719	1.3694	2 3708	4 8059	4 2053	7.4006	12.5401
PMMA	Methyl Alcohol	Teflon	2.7284	2 5719	1.3754	2 3708	4 7108	4 2053	7.3388	12.5401
Copper	NM	Teflon	2.1438	2.0103	0.2524	0.4294	2.6591	2.606	1.4351	2.5144
Copper	Water	Teflon	1 8502	2.0103	0.1954	0 4294	2 5748	2.606	1.241	2.5144

* 1 refers to the case when the attenuator shock pressure (at the "exit") is 2 GPa, 2 refers to the case with 10 GPa

The program can handle the following attenuators: Copper, PMMA, 2024 Al, 921-T Al, Teflon
The program can handle the following test liquids: NM, water, ethyl alcohol, methyl alcohol, acetone
The program can handle the following container materials: Teflon, nylon, polyethylene, polystyrene, polyurethane, PVC, lead, rubber